DESIGN AND ANALYSIS OF A MECHANICAL DRIVE UNIT WITH TWO DEGREES OF FREEDOM

A Thesis Submitted
in Partial Fulfilment of the Requirements
for the Degree of

MASTER OF TECHNOLOGY

By

MAGANTY SATYA PRASAD

to the

DEPARTMENT OF MECHANICAL ENGINEERING

INDIAN INSTITUTE OF TECHNOLOGY KANPUR

JULY, 1983

ME-1983-M-PRA-DES

C E R T I F I C A T E

This is to certify that the present work ''Design and Analysis of a Mechanical Drive Unit with two Degrees of Freedom'' has been carried out under our supervision and has not been submitted elsewhere for the award of a degree.

A. Ghosh
Professor
Dept. of Mech. Eng.
I.I.T. Kanpur
INDIA.

K.C. Pande
Professor
Dept. of Mech. Eng.
I.I.T. Kanpur
INDIA.

July, 1983.

A C K N O W L E D G E M E N T

The author wishes to express his deep sense of gratitude and appreciation to his advisors Dr. A. Ghosh and Dr. K.C. Pande, who have guided this work from conception to completion.

The author would like to thank his friends Messers A.V.V. Satyanarayana, P.V. Rao, E.S. Reddy, V. Raghuram, M. Gopi Krishna and Chandrasekar for their timely help provided whenever necessary.

The author also expresses his appreciation to Mr. Bhartiya and Mr. M.M. Singh for rendering their services in fabricating the experimental set-up.

Thanks are also due to Mr. J.P. Gupta, Mr. Qasim and Mr. Laltha Prasad to produce the work in the present form.

M.S. PRASAD

C O N T E N T S

			Page
CERTIFICATE			ii
ACKNOWLEDGEMENT			iii
LIST OF FIGURES			v
NOMENCLATURE			viii
SYNOPSIS			xii
CHAPTER 1	:	INTRODUCTION	1
1.1		Mechanical Variable Speed Drives	2
1.2		Hydraulic Variable Speed Drives	6
1.3		Electrical Variable Speed Drives	12
1.4		Controlled Differential Drives	14
1.5		Objective and Scope of the Present Work	15
CHAPTER 2	:	DEVELOPMENT AND THEORETICAL ANALYSIS	18
2.1		Differential Gear-Ball Governor System	20
2.2		Differential Gear-Paddle System	48
2.3		Differential Gear-DC Shunt Generator System	56
CHAPTER 3	:	EXPERIMENTAL INVESTIGATION	62
3.1		Experimental Set-up	62
3.2		Results and Discussion	65
CHAPTER 4	:	SUMMARY AND CONCLUSIONS	68
REFERENCES			70

LIST OF FIGURES

FIGURE NO.		PAGE
1.1	Four basic belt arrangements for varying output speed	4
1.2	Some basic arrangements in variable speed cone drives	7
1.3	Schematic sketch of a variable speed disk drive	8
1.4	Variable speed ring drive	8
1.5	Schematic sketch of variable speed spherical drive	8
1.6	Variable speed multiple disk drive	9
1.7	Variable speed impulse drive (Zero-max drive)	9
1.8	Scoop type variator - a hydrodynamic drive	11
1.9	Hydroviscous drives (a) electro-viscous hydraulic clutch (b) liquid slip clutch	11
1.10	Schematic sketch of variable speed hydrostatic drive	13
1.11	Schematic sketch of controlled differential drive	16
2.1	Schematic illustration of the proposed concept	19
2.2	Schematic diagram of differential gear-ball governor system	21
2.3	Schematic diagram of the differential gear unit	25
2.4	Free body diagrams of (a) governor ball (c) governor sleeve	25

FIGURE NO.		PAGE
2.5	Effect of step ratio R on the system characteristics	28
2.6	Effect of governor ball mass m_b on the system characteristics	29
2.7	Effect of spring stiffness k on the system characteristics	30
2.8	Free body diagrams of (a) Output shaft with output bevel gear (b) (b) Planet carrier	32
2.9	Free body diagrams of (a) upper planet gear (b) lower planet gear	
2.10	Variation of system time constant with governor ball mass for different output loads	45
2.11	Variation of system time constant with governor ball mass for different sleeve positions	46
2.12	System response to step change in sleeve position	49
2.13	System response to step change in output load	50
2.14	Schematic diagram of differential gear-paddle system	51
2.15	Effect of step ratio R on the $\omega_o - B_w$ characteristics of the system	54
2.16	Effect of step ratio R on the $\omega_o - T_o$ characteristics of the system	55
2.17	Effect of the parameter d/D_t on the $\omega_o - B_w$ characteristics of the system	57
2.18	Effect of the parameter d/D_t on the $\omega_o - T_o$ characteristics of the system	58
2.19	Equivalent circuit diagram during steady state operation	59

FIGURE NO.		PAGE
2.20	Effect of step ratio R on the $\omega_o - R_L$ characteristics of the system	61
3.1	Schematic sketch of the experimental set-up	63
3.2	Photograph of the experimental set-up	64
3.3	Experimental $\omega_o - R_L$ characteristics of the system	67

N O M E N C L A T U R E

B_w	Baffle width
b	Width of the paddle
b_i, b_o, b_r b_c, b_1, b_2	Viscous damping coefficients in the bearings
C_{Re}	Critical Reynold's Number
D_t	Mixing tank diameter
d	Paddle diameter
E	E.M.F. generated
e	Eccentricity of the sleeve of the ball governor
$\bar{F}$	Force vector acting on the upper planet gear
f_o	Initial compression force in the spring of the ball governor
g	Acceleration due to gravity
$\bar{H}$	Angular momentum vector of the upper planet about the origin of xyz axes
h	Height of the liquid column in the mixing tank
I_a	Armature current
I_f	Field current
I_L	Load current
I_i	Moment of inertia of the input shaft with the input bevel gear about the axis of rotation
I_o	Moment of inertia of the output shaft with the output bevel gear about the axis of rotation

I_r	Moment of inertia of the planet carrier about the axis of rotation
I_{px}, I_{py}, I_{pz}	Moment of inertia of the planet bevel gear about the x, y and z axis, respectively
I_1	Moment of inertia of the control shaft assembly
I_2	Moment of inertia of the intermediate shaft assembly
k	Spring stiffness of the ball governor
ℓ	Length of the links of the ball governor
$\bar{M}$	Moment vector about the origin of xyz axes of the upper planet gear
M_{R1x}, M_{R1y}; M_{R2x}, M_{R2y}	Moment components exerted by the pin on the upper and lower planet gears, respectively
m_s	Mass of the sleeve of the governor
m_b	Mass of the governor ball
m_p	Mass of the planet bevel gear
N_{1t}, N_{1r}, N_{1a}; N_{2t}, N_{2r}, N_{2a}	Force components exerted by the upper and lower planets on the input bevel gear, respectively
N_{pmax}	Power number under fully baffled condition
N_p	Power number under partially baffled condition
$N_{p\infty}$	Power number at infinite Reynold's Number
n	Number of baffles
P_{1t}, P_{1r}, P_{1a}; P_{2t}, P_{2r}, P_{2a}	Force components exerted by the upper and lower planets on the output bevel gear, respectively

P	Power consumed in the mixing vessel
p	Contact pressure at the sleeve-stopper interfa
Q_t, Q_r, Q_a	Force components exerted by the pinion on the crown wheel attached to the planet carrier
R	Net gear ratio between the planet carrier and the control device
$R_{1t}; R_{1r}, R_{1a};$ R_{2t}, R_{2r}, R_{2a}	Force components exerted by the pin on the upper and lower planets, respectively.
r	Radius of operation of the ball governor
r_b	Radius of governor ball
r_f	Radius of application of the stopper
r_{pi}	Pitch circle radius of the input bevel gear
r_{po}	Pitch circle radius of the output bevel gear
r_{pr}	Pitch circle radius of the crown wheel
r_{pp}	Pitch circle radius of the planet bevel gear
r_{pp1}	Pitch circle radius of the pinion
r_{pp2}	Pitch circle radius of the pulley 6
r_{pp3}	Pitch circle radius of the pulley 7
r_{pp4}	Pitch circle radius of the pulley 8
r_{pp5}	Pitch circle radius of the pulley 9
S_1, S_2	Tension in the links of the ball governor
T_i	Input torque
T_o	Output load torque

T_r	Torque available at the crown wheel
T_c	Torque available at the control device
T_f	Friction torque provided by the ball governor
x	Movement of the sleeve from its lowest position
ω_i	Angular velocity of the input shaft
ω_o	Angular velocity of the output shaft
ω_r	Angular velocity of the planet carrier
ω_c	Angular velocity of the control device shaft
ω_p	Spin rate of the planet gear relative to xyz system
ω_{xyz}	Angular velocity of xyz axes
ω	Absolute angular velocity of the upper planet
ρ	Density of the fluid in the mixing paddle
μ	Coefficient of friction at the sleeve-stopper interface
τ	System time constant
i,j,k	Unit vectors along xyz axes, respectively

S Y N O P S I S

DESIGN AND ANALYSIS OF A MECHANICAL DRIVE UNIT WITH TWO DEGREES OF FREEDOM

A Thesis Submitted
In Partial Fulfilment of the Requirements
for the Degree of

MASTER OF TECHNOLOGY

by

MAGANTY SATYA PRASAD

to the

DEPARTMENT OF MECHANICAL ENGINEERING
INDIAN INSTITUTE OF TECHNOLOGY KANPUR

JULY, 1983

Development of a continuous variable speed mechanical drive is presented. A concept employing a mechanical differential and a dissipative control device is proposed. Theoretical feasibility of using a ball governor, a mixing paddle and a dc shunt generator as control devices is analyzed. An experiment using the dc shunt generator as the control device is conducted to establish the validity of the concept.

CHAPTER 1

INTRODUCTION

Several power applications require drives that can produce a large number of speed ratios or even an infinite number of speed ratios. The class of transmission devices providing certain predetermined fixed speed ratios, such as gear boxes, stepped pulleys and common chain drives may be referred to as stepped methods of speed adjustment. Continuously variable speed devices, on the other hand, are mechanisms which convert a constant input speed into output speeds which are steplessly variable within a certain range. This range may cover a definite ratio of maximum to minimum output speeds, or it may reach from a maximum output speed right down to zero. Such devices where the output speed can be reduced to zero are called infinitely variable speed drives. In some cases the direction of rotation of the output shaft can also be changed without changing the direction of rotation of the input member.

Infinitely variable speed drives are commonly empolyed (a) in manufacturing processes to ensure optimum production rates with variations in raw materials, (b) for providing constant cutting speeds in machine tools in accordance with varying work diameters, (c) for compensating the effects of viscosity, temperature and humidity in

processing plants, (d) for synchronizing the flow of material from one machine to another and (e) in unconventional machining operations such as electro-discharge machining.

Variable speed drive requirements may be met by means of mechanical, hydraulic or electrical devices. The principle of operation of each type of variator is briefly discussed in the next few sections.

1.1 MECHANICAL VARIABLE SPEED DRIVES

Variable speed mechanical drives [1,2] can be grouped into four major classes based upon their operating principle :

(a) Belt drives

(b) Chain drives

(c) Friction drives :- subclassified into

- Cone drives
- Disk drives
- Ring drives
- Spherical drives
- Multiple disk drives

(d) Impulse drives.

Belt drives : Majority of the low horsepower applications requiring variable speed drives can be satisfied by the use of variable speed belt drive systems because of their simplicity and low initial cost. On the other hand, all such systems

have certain shortcomings which may rule them out for certain specialized applications. Among these shortcomings, which are present to some degree in practically all these drives, is the fact that the speed is not maintained strictly constant under varying and shock loads due to slip and belt stretch. But this slippage is small when compared to that in friction drives. Further, because of the wear of the belt they are not suitable for constant power applications. Speed adjustment in belt drives is obtained through four basic arrangements : (i) drives employing one variable pitch pulley driving one fixed pulley or vice versa (Fig. 1.1a), (ii) drives employing variable pitch pulleys on both input and output shafts maintaining constant centre distance (Fig. 1.1b), (iii) drives employing solid sheaves on both input and output shafts with variable pitch pulleys on the intermediate shafts (Fig. 1.1c), and (iv) drives with co-axial input and output shafts with all variable pitch pulleys (Fig. 1.1d). In variable speed belt drives the rotating member (sheave) has to be moved in order to affect speed adjustment.

Chain drives : Chain drives maintain fixed phase relationship between the input and output shafts. In these drives the basic arrangement for obtaining speed ratios is similar to that in belt drives except that the chain runs in radially grooved faces of conical surface sheaves which are located on the input and output shafts. The faces are not straight

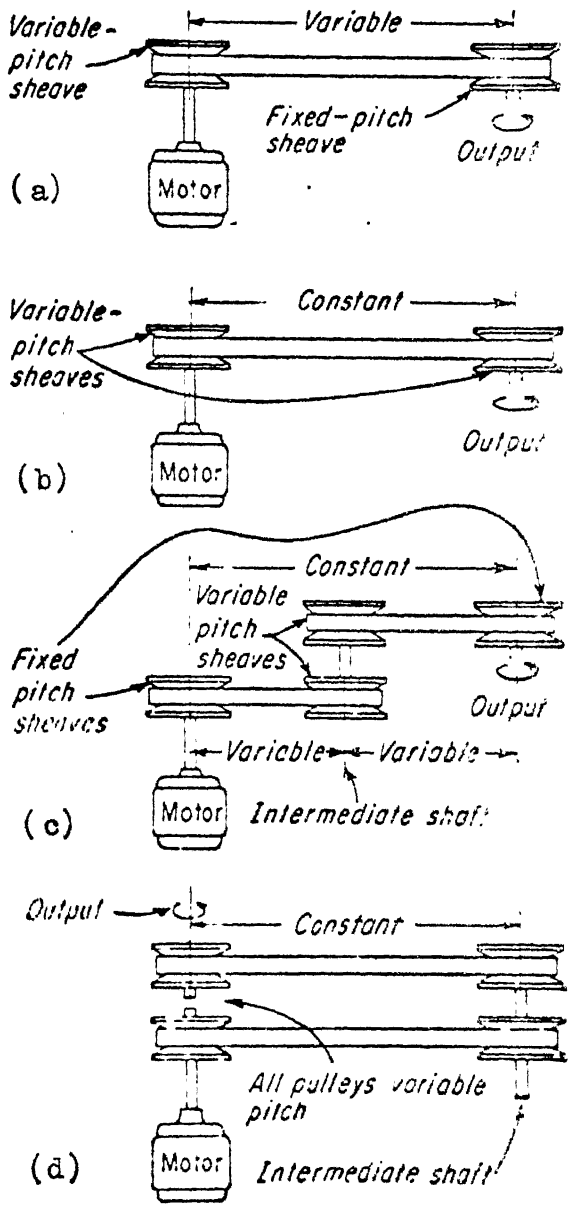

Fig. 1.1 : Four basic belt arrangements for varying output speed.

cones, but have a slight convex curve to maintain proper chain tension at all positions. The pitch diameters of the sheaves are varied in order to achieve speed adjustment.

Friction drives : The distinguishing feature of friction drives is that rotary motion is transmitted from one rotating part to another rotating part by friction generated through a point or line of contact. Speed changes are then possible by altering the position of the point or line of contact relative to the centres of rotation of the driving and the driven members. In practice, the majority of friction drives employ intermediate points (or lines) of contact in series. These intermediate members may be cones, disks, rings, balls etc. and correspondingly they are known as cone drives, disk drives, ring drives, spherical drives. In all friction drives the transmissible power depends on the magnitude of frictional drag, which in turn, depends on the contact pressure applied. This pressure must be undesirably large in order to transmit large powers. Alternatively, provision must be made for multiplicity of contact points (or lines) in parallel with each other, each carrying part of the total load to be transmitted. To obtain multiplicity of contact points (or lines) the number of intermediate members must be increased resulting in design complications and higher costs. Speed adjustment in friction drives is accomplished by moving the rotating intermediate member or members. Figures 1.2 to 1.6

illustrate the operating principle of cone drives, disk drives, ring drives, spherical drives and multiple disk drives, respectively.

Impulse drives : In these drives, the driving member rotates on eccentric which through the linkage causes the output link to rotate through a fixed amount. On the return stroke, the output link overrides the output shaft. Thus a pulsating motion is transmitted to the cutput shaft. Shifting the adjustable pivot varies the speed ratio. By adding eccentrics, cranks and clutches in the system, the frequency of pulsations per revolution can be increased to produce a smoother drive. This class of drives are mainly suitable for fractional horsepower applications. Fig. 1.7 illustrates the operating principle of zero-max drive belonging to this class of drives.

1.2 HYDRAULIC VARIABLE SPEED DRIVES

Variable speed hydraulic drives [3] are broadly classified into :

(a) Hydrodynamic drives
(b) Hydroviscous drives
(c) Hydrostatic drives.

Hydrodynamic drives : The operating principle of this class of drives is that the kinetic energy of hydraulic fluid, set in motion by the input impeller, drives the output impeller

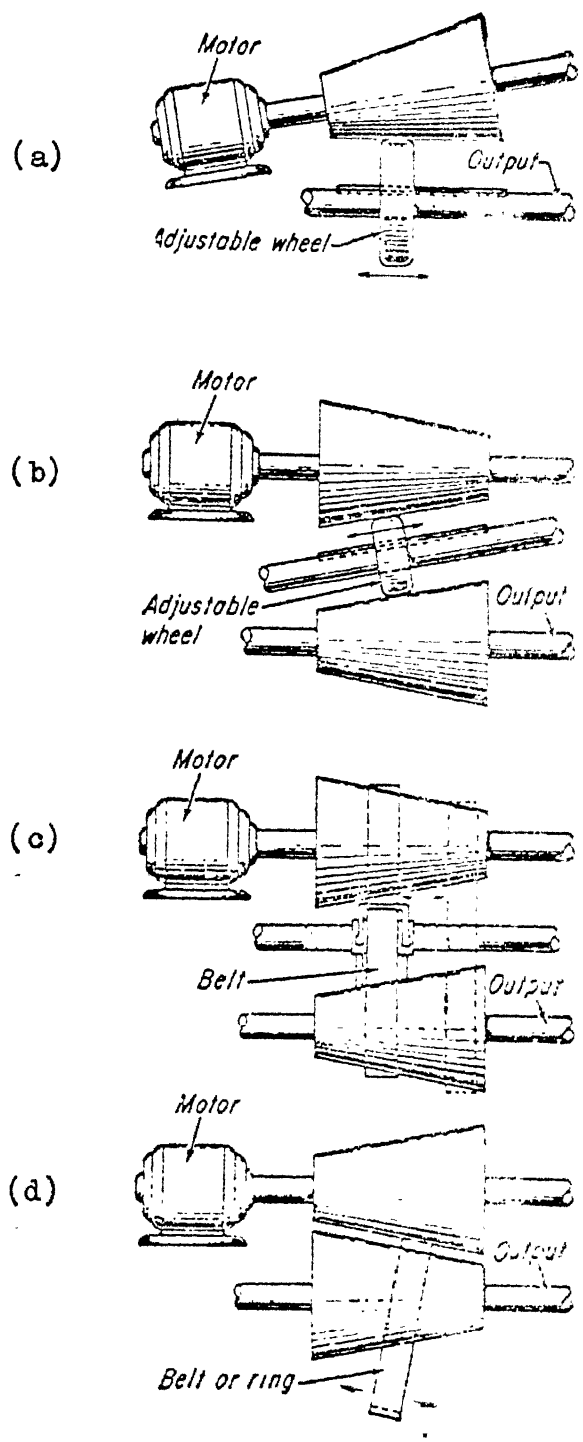

Fig. 1.2 : Some basic arrangements in variable speed cone drives.

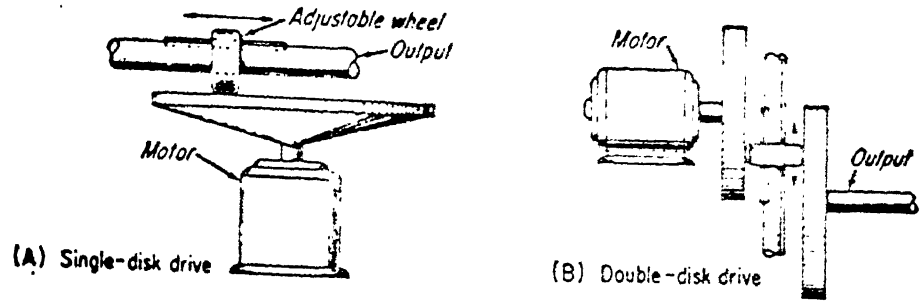

Fig. 1.3 : Schematic sketch of a variable speed disk drive.

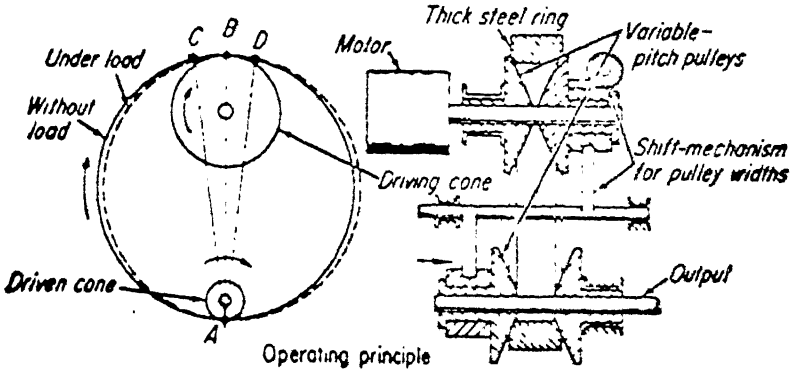

Fig. 1.4 : Variable speed ring drive.

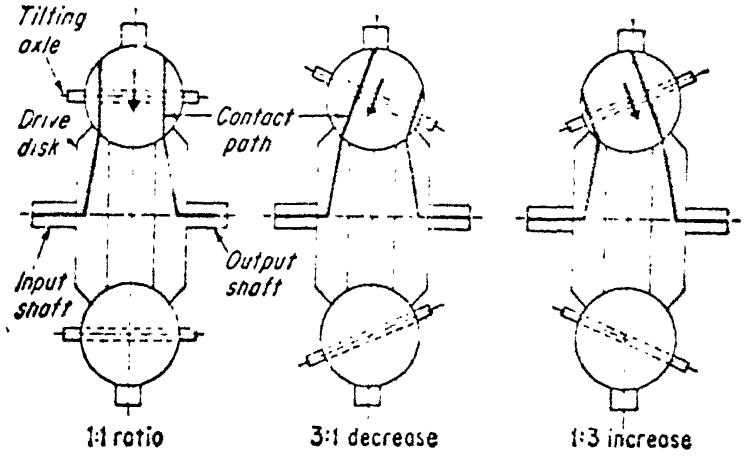

Fig. 1.5 : Schematic sketch of variable speed spheroid drive.

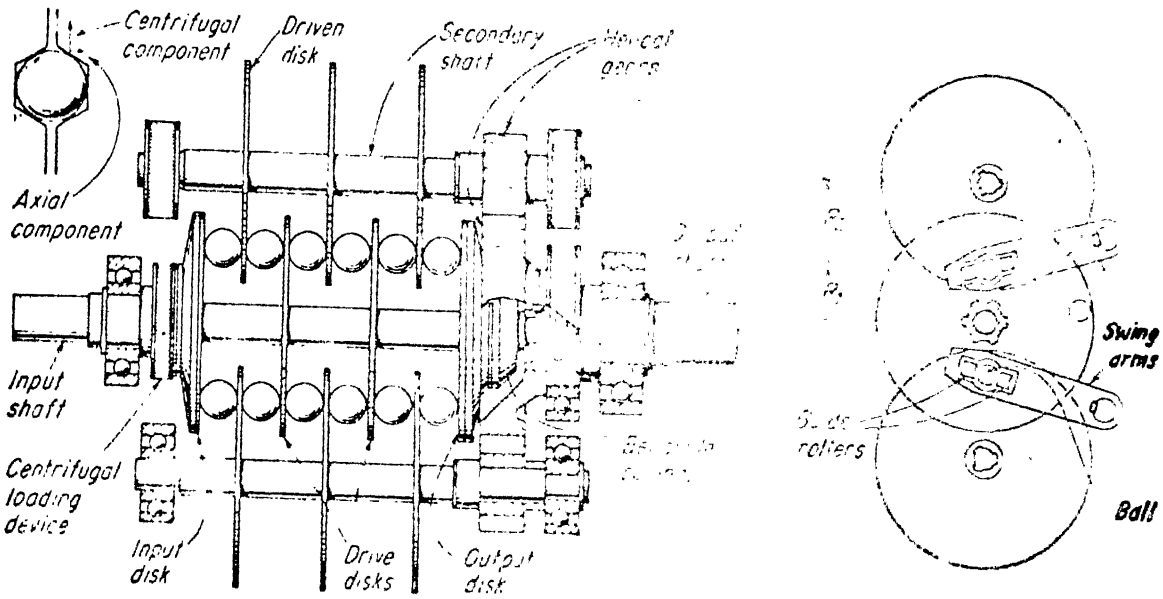

Fig. 1.6 : Variable speed multiple disk drive.

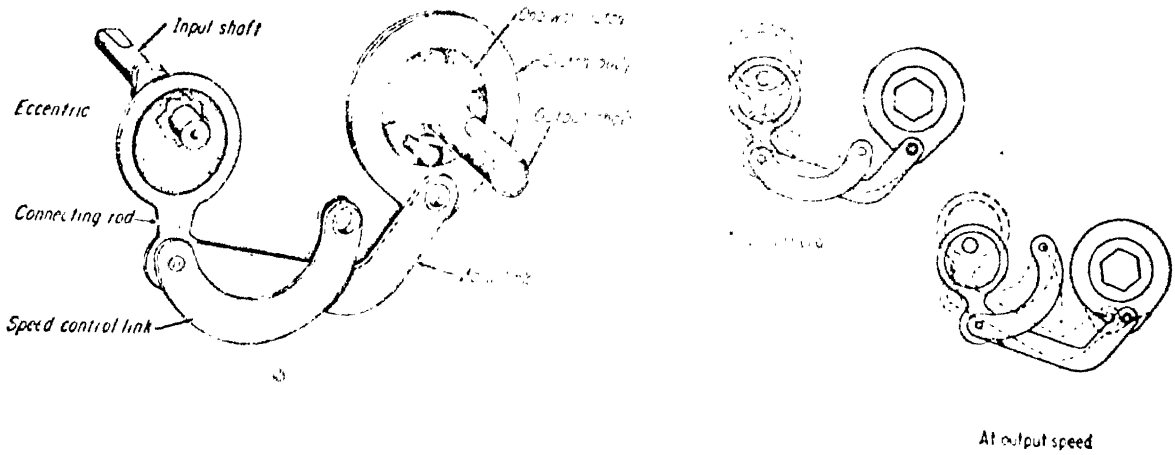

Fig. 1.7 : Variable speed impulse drive (Zero-max drive).

(runner). Scoop-type of hydraulic variator belonging to this class of drives is shown in Fig.1.8. Speed adjustment can be obtained by varying the volume of oil through nozzle E, tending to empty the casing B. However, Scoop tube F prevents this by scooping up the oil and returning it to the drive casing. The disadvantage with this type of drives is that they are not suitable for constant speed operations with varying load. In these drives also the rotating member has to be moved in order to affect speed changes.

Hydroviscous drives : Speed control in these drives is affected through changes in viscosity of the fluid. In electroviscous hydraulic clutch (Fig. 1.9a), viscosity of the oil is changed by the electric potential applied across it. In liquid slip clutch (Fig. 1.9b), the thickness of the fluid film is varied to affect speed adjustment. In these drives cooling arrangement has to be provided to remove the heat generated. In some drives of this class (liquid slip clutch) the rotating member has to be moved to achieve speed adjustment.

Hydrostatic drives : Hydrostatic drive consists of a positive-displacement pump driving a positive displacement fluid motor usually in one of the following basic arrangements.

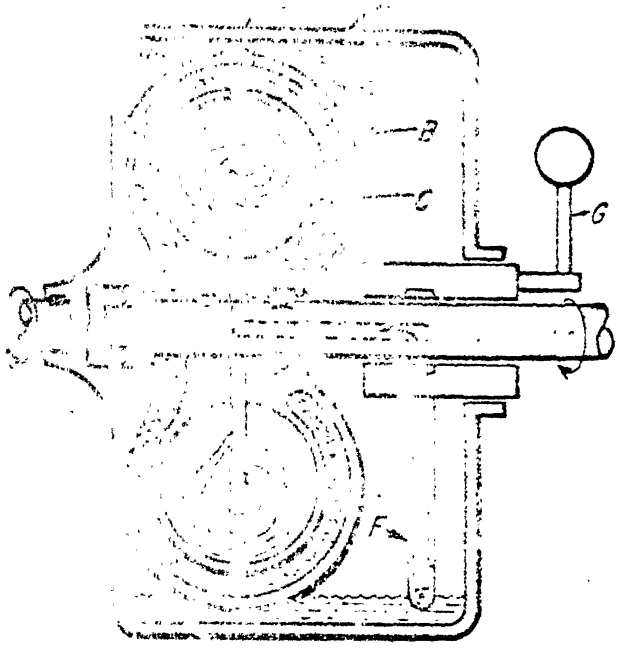

Fig. 1.8 : Scoop type variator - a hydrodynamic drive.

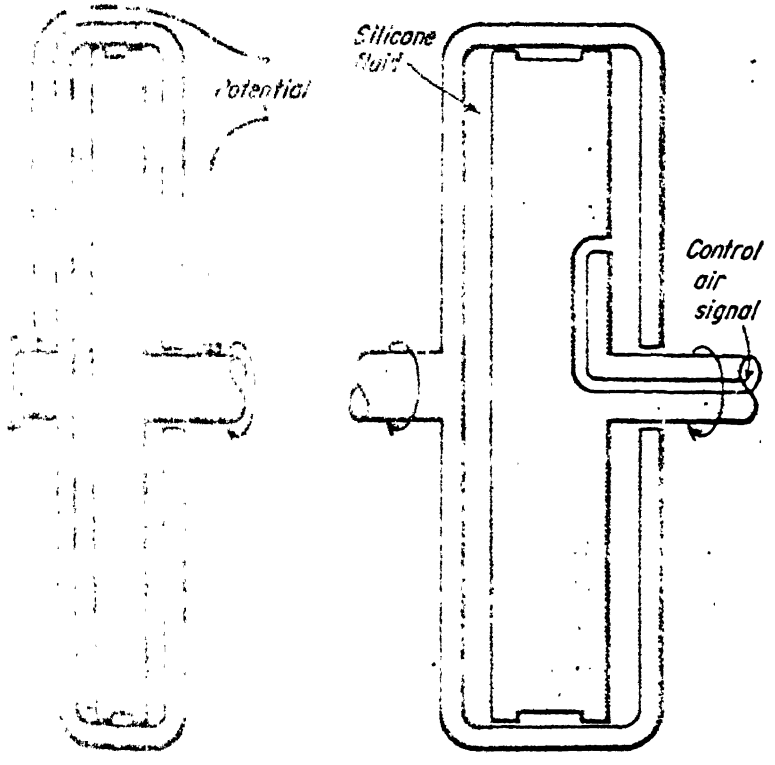

Fig. 1.9 : Hydrodynamic drives (a) Electro-viscous clutch, (b) liquid slip clutch.

(a) PF-MF (with flow control valves) : Fixed displacement pump and a fixed displacement motor (Fig. 1.10a). Motor speed is adjusted by controlling the input or output flow of the motor.

(b) PF-MV : Fixed displacement pump and variable displacement motor (Fig. 1.10b). Motor speed is adjusted by changing the effective stroke of the piston or vanes.

(c) PV-MF : Variable displacement pump and fixed displacement motor (Fig. 1.10c). Motor speed is adjusted by varying the pump displacement to vary pump flow.

(d) PV-MV : Variable displacement pump and variable displacement motor (Fig. 1.10d). Motor speed is adjusted by a combination of adjustments of pump and motor displacements.

1.3 ELECTRICAL VARIABLE SPEED DRIVES

Variable speed electrical drives [4,5] can be of either a.c. or d.c. types. Two of these drives, namely, the Ward-Leonard system and eddy-current clutch are discussed here.

Ward-Leonard system : In this drive, the generator coupled to the input shaft generates a dc voltage which is fed to a dc variable speed motor. Speed control of dc motor is achieved by controlling the field voltage of the generator or by controlling the field voltage of the dc motor itself (if it is used

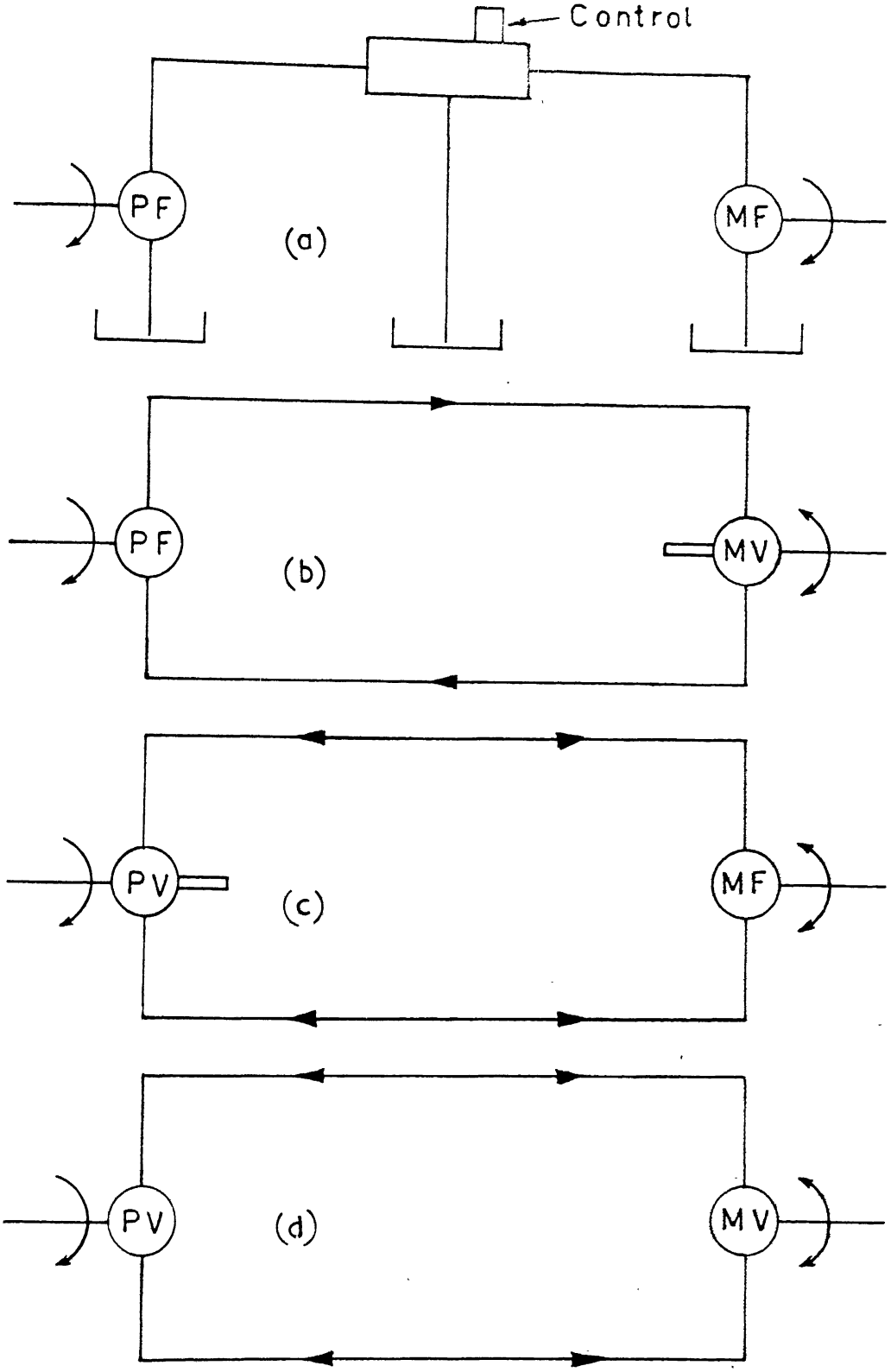

FIG.1·10 SCHEMATIC SKETCH OF VARIABLE SPEED HYDROSTATIC DRIVE.

as separately excited). Weakening the field of the dc motor speeds up the output speed whereas weakening the field of the generator decreases the output speed of the dc motor.

Eddy-current clutch : The eddy-current clutch has two main elements, a drum and an inside spider. The drum is driven by the input shaft, whereas the speed of the spider is adjustable. The field coil energized with dc is usually stationary. The spider is magnetized by the field coil and acts as salient poles of a generator. When the drum rotates it passes north and south poles of the spider inducing eddy-currents. The combined action of current and flux develops the electromagnetic torque. Speed of the drive is controlled by varying the field current.

1.4 CONTROLLED DIFFERENTIAL DRIVES

The power and speed characteristics of any variable speed drive (either mechanical, hydraulic or electrical) may be altered by suitably coupling it to a differential gear unit. Such drive arrangements are known as controlled differential drives [1].

The configuration shown in Fig. 1.11a results in an increase of the horsepower range but decreases the output speed range.

Output speed $n_4 = \frac{1}{2}\left(n_1 + \frac{n_2}{R_1}\right)$

where $R_1 > 1$.

Output torque $T_4 = 2T_3 = 2R_1T_2$.

Output horsepower $= T_2 (n_1R_1 + n_2)\ 2\pi/746$.

Hoursepower increase $= T_2R_1n_1 \cdot 2\pi/746$.

Output speed range $= n_{4max} - n_{4min} = \frac{1}{2R_1}(n_{2max} - n_{2min})$.

Thus, the horsepower range is increased while the output speed range decreases.

To increase the output speed range at the cost of a reduction in the horsepower transmitted, the arrangement shown in Fig. 1.11b may be employed:

Output speed $n_4 = \frac{1}{2}(n_2 \pm n_3)$.

Output speed range $= n_{4max} - n_{4min} = \frac{1}{2}(n_{2max} - n_{2min}) + R_1n_1$.

Reduction in hp $= T_2 \cdot n_3 \cdot 2\pi/746$.

Thus, the speed range is increased at the expense of horsepower range.

1.5 OBJECTIVE AND SCOPE OF THE PRESENT WORK

The development of a mechanical variable speed drive system capable of good speed control characteristics and possessing low output speed sensitivity to output load torque changes forms the topic of the thesis. A system incorporating the mechanical differential gear unit (a two degree of freedom system) and a dissipative control device is proposed to achieve

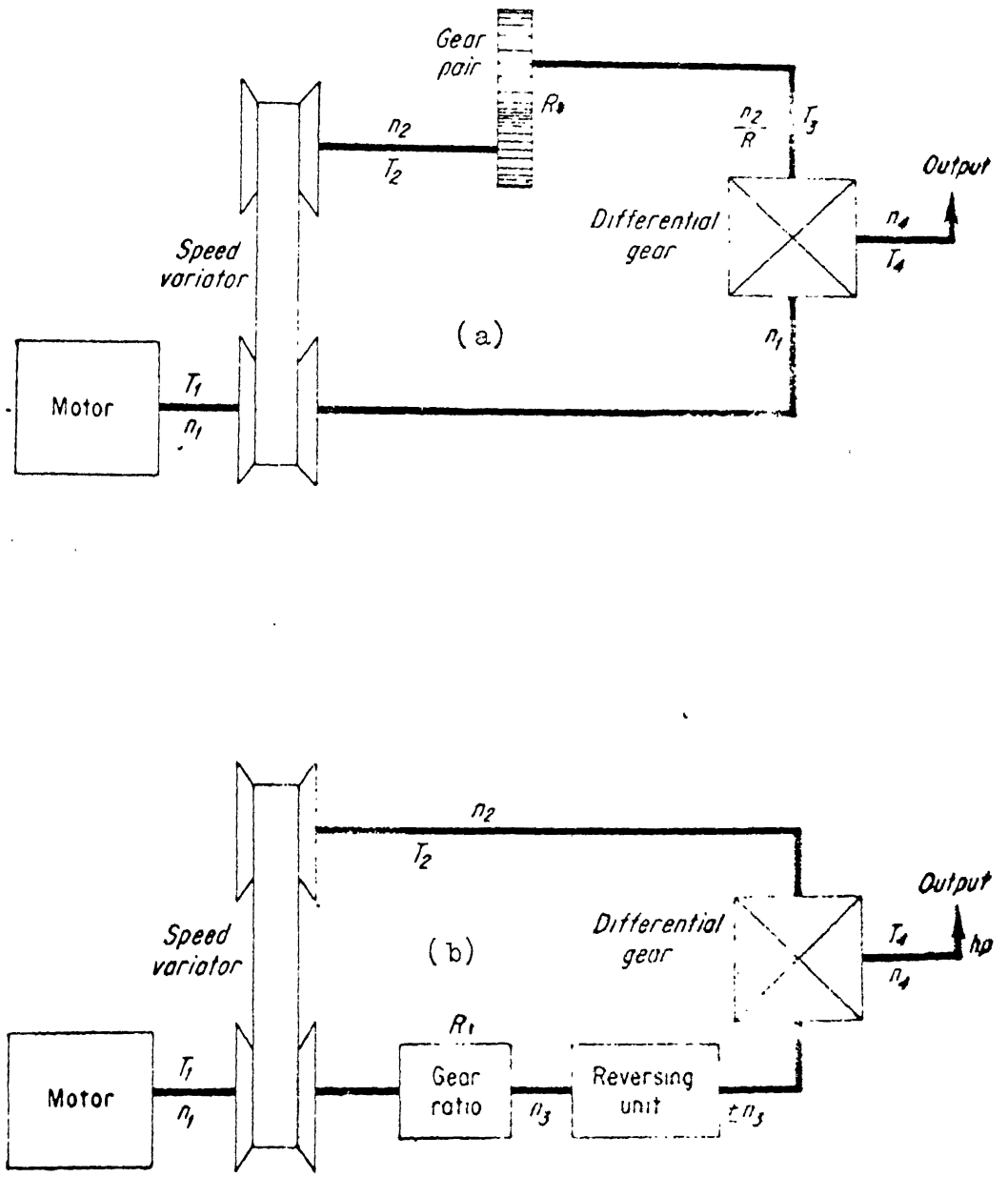

Fig. 1.11 : Schematic sketch of controlled differential drive.

the present objective. The potential of using three different physical systems, namely, (i) a ball governor (ii) a mixing paddle and (iii) a dc shunt generator for possible utilization as the control device is studied through a detailed analysis. An experiment is carried out using the dc shunt generator as the control device to evaluate the practical feasibility of the proposed concept.

CHAPTER 2

DEVELOPMENT AND THEORETICAL ANALYSIS

The proposed concept is illustrated schematically in Fig.2.1. The constant input speed ω_i forms the input to the differential. One output O_1 of the differential forms the output ω_o of the system. The other output O_2 running at speed ω_r is connected to the control device. In steady state operation, for given values of ω_o and T_o, the control speed ω_r and the control torque T_r will assume certain specific values. As is well known, the angular speeds ω_i, ω_o and ω_r are kinematically related. With the input speed ω_i constant, changes in the control shaft speed ω_r will be reflected in the output speed ω_o. In steady state, the control shaft torque T_r is determined by the output load torque T_o. Thus it is apparent that, if the control device could be run at different speeds ω_r for the same applied torque T_r, any desired values of ω_o may be achieved. This would be possible if the control device provides a resisting torque, equal to T_r in steady state, which is a function of ω_r and some adjustable control device parameter. By adjusting the control device parameter, the system output speed ω_o may thus be varied.

The amount of power dissipated in the control device is given by $T_r \omega_r$. Adjusting the control device parameter alters ω_r and hence the energy dissipation. The infinitely

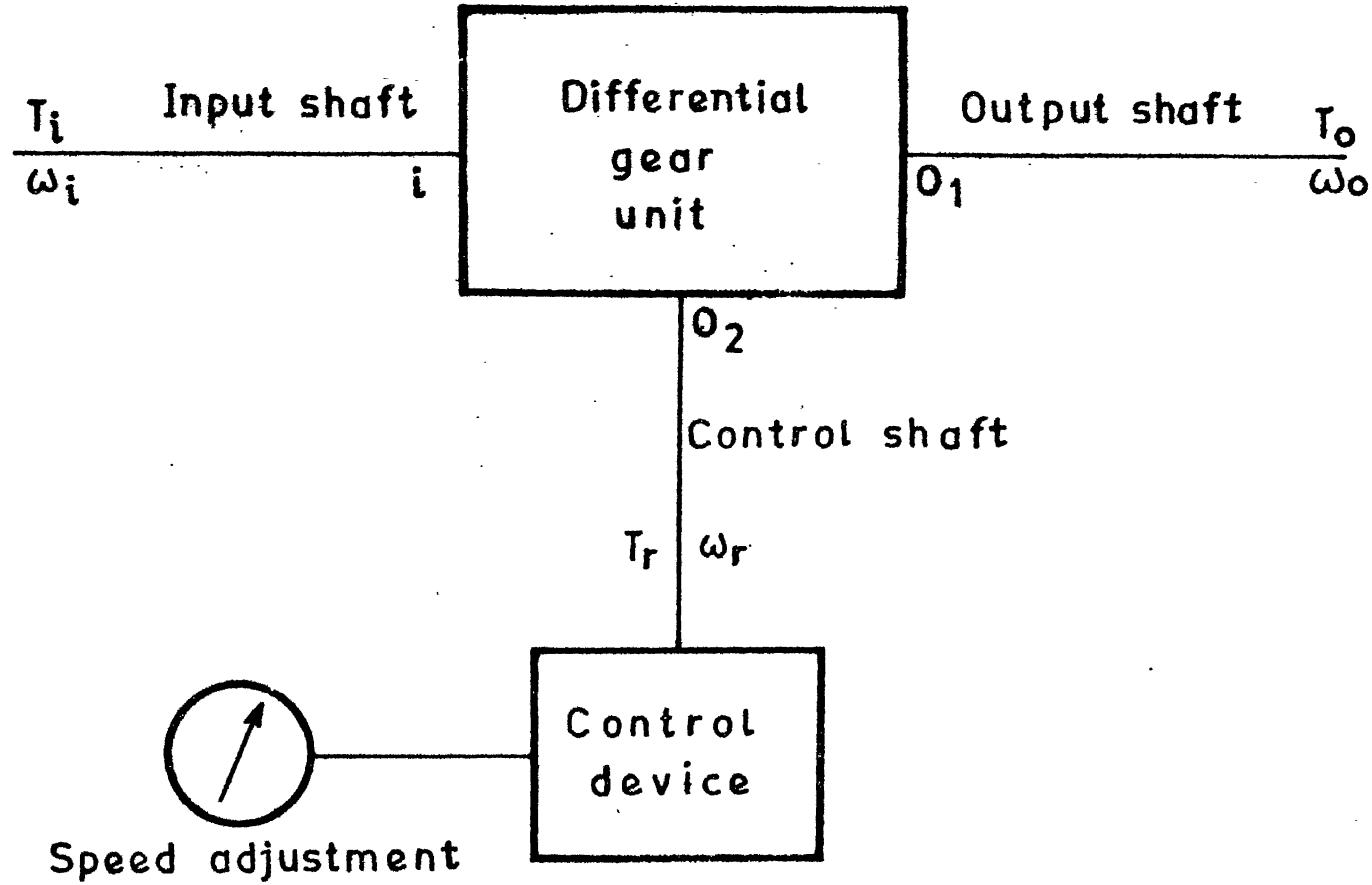

FIG.2.1 SCHEMATIC ILLUSTRATION OF THE PROPOSED CONCEPT.

variable output speed is therefore achieved by continuously dissipating a part of the power supplied by the input shaft. The concept would thus be practical only for low power applications where the energy dissipation would be small.

A comment concerning the size of the control device would be significant. Incorporating a speed step up between the control shaft and the control device, the latter would be required to offer a smaller resisting torque although running at a higher speed. This would help to reduce the size of the control device.

In the analysis to follow, the feasibility of using three different physical systems, namely, a ball governor, a mixing paddle and a dc shunt generator as control devices is studied. The steady state characteristics of the complete differential gear-control device system are determined in each case. The dynamic behaviour is also analyzed for the case of the differential gear-ball governor system.

2.1 DIFFERENTIAL GEAR-BALL GOVERNOR SYSTEM

The schematic sketch of the variable speed drive employing the ball governor as the controlling device is shown in Fig. 2.2. One of the outputs from the differential drives the output load, and the control output, after step-up, drives the ball governor. The sleeve of the spring-loaded ball governor rubs against a stopper and dissipates energy in the form of heat. The output speed changes are affected by the movement of the stopper.

1. Input Bevel Gear
2. Output Bevel Gear
3. Planet Bevel Gear
4. Crown Wheel
5. Bevel Pinion
6-9. Pulley system
10. Stopper

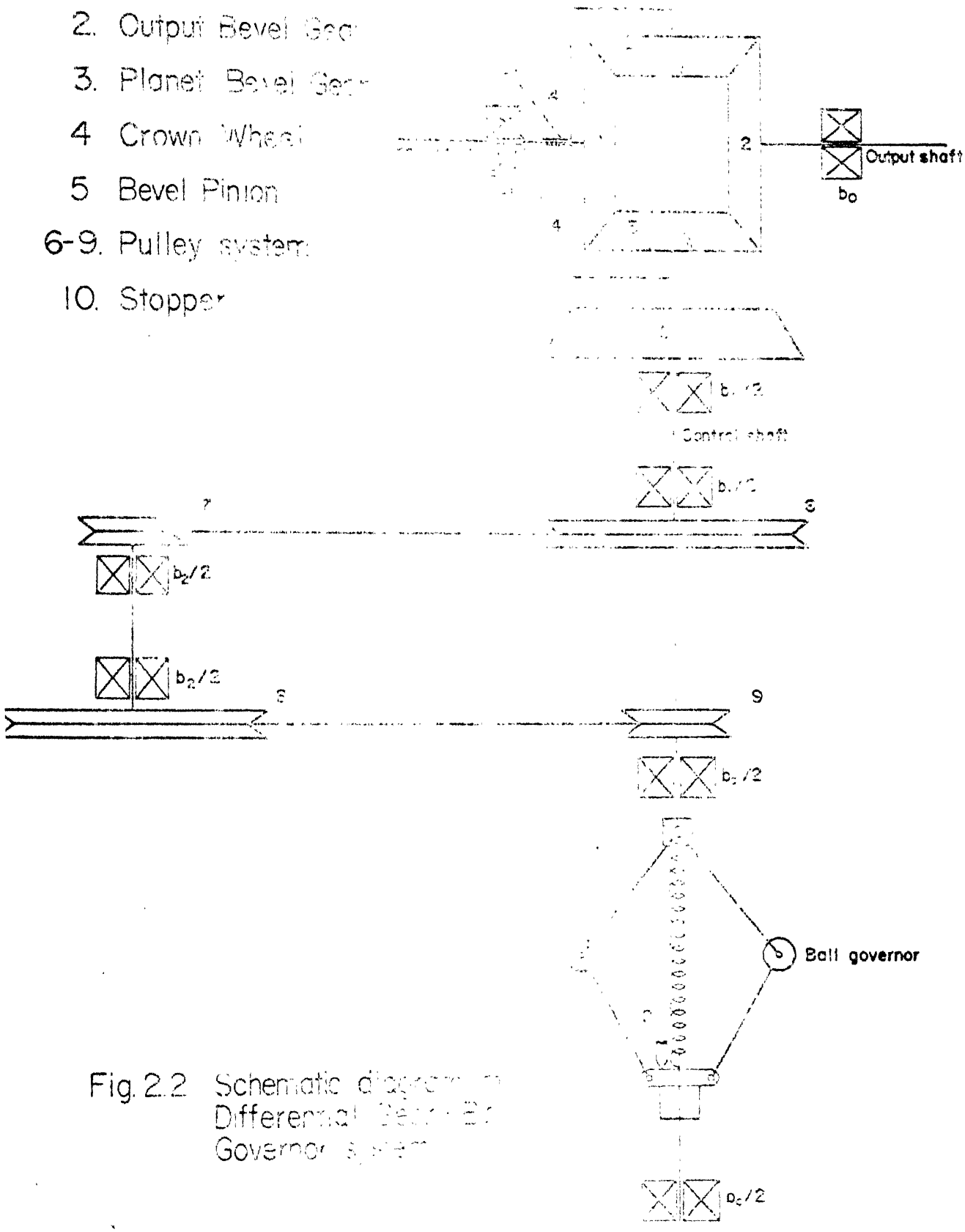

Fig. 2.2 Schematic diagram of Differential Gear Box Governor system

2.1.1 Steady State Analysis

Fig. 2.3 shows a view of the differential indicating the external torques acting about the axis of rotation. Using no slip condition at points A and B, the following two kinematical relations may be written,

$$r_{pi}\,\omega_i = r_{po}\,\omega_r + r_{pp}\,\omega_p \qquad (2.1)$$

$$r_{po}\,\omega_o = -r_{pi}\,\omega_r + r_{pp}\,\omega_p \,. \qquad (2.2)$$

Eliminating ω_p from equations (2.1) and (2.2), the kinematical relation between the input speed, output speed and the control speed is,

$$\omega_o = \omega_i - 2\omega_r \,. \qquad (2.3)$$

Also, we have,

$$\omega_c = R\,\omega_r \,. \qquad (2.4)$$

From equations (2.3) and (2.4), the governor speed ω_c is related to the output speed ω_o as,

$$\omega_c = \frac{R}{2}(\omega_i - \omega_o) \,. \qquad (2.5)$$

The sum of external torques should be zero for no angular acceleration about the axis of rotation,

$$T_i - b_i\omega_i + T_o + b_o\,\omega_o - T_r - b_r(\omega_i - \omega_r) = 0 \,. \qquad (2.6)$$

Further, for energy balance the following expression must be satisfied:

$$T_i\omega_i = T_o\omega_o + T_r\omega_r + b_i\omega_i^2 + b_o\omega_o^2 + b_r(\omega_i - \omega_r)\omega_i \quad . \tag{2.7}$$

Solving for T_i and T_r as a function of T_o and ω_o from equations (2.3), (2.6) and (2.7), we obtain,

$$T_i = T_o + b_i \frac{(2\omega_i^2 + \omega_o^2 - \omega_i\omega_o)}{(\omega_i + \omega_o)} + b_o \frac{\omega_o(\omega_i + 2\omega_o)}{(\omega_i + \omega_o)} + \frac{b_r}{2}(\omega_i + \omega_o) \tag{2.8}$$

$$T_r = 2T_o + b_i \frac{(\omega_i - \omega_o)^2}{(\omega_i + \omega_o)} + b_o \frac{\omega_o(2\omega_i + 3\omega_o)}{(\omega_i + \omega_o)} \tag{2.9}$$

and

$$T_c = T_r/R \quad . \tag{2.10}$$

Note that, when the viscous damping in the bearings is negligible, the input torque is equal to the output torque and the torque available at the planet carrier T_r is twice the output torque T_o (familiar feature of automotive rear axle differential where equal torque is transmitted to the two rear axles irrespective of their speeds).

Next, consider the free body diagrams of the governor ball and the sleeve shown in Figs. 2.4a and 2.4b, respectively. The following equations of motion may be easily written:

$$S_1 \sin \alpha + S_2 \sin \beta = m_b r \omega_c^2 \qquad (2.11a)$$

$$S_1 \cos \alpha - S_2 \cos \beta - m_b g = 0 \qquad (2.11b)$$

$$p - 2 S_2 \cos \beta - kx - f_o = 0 \ . \qquad (2.11c)$$

The frictional torque developed at the sleeve-stopper interface may be expressed as,

$$T_f = \mu r_f p \ . \qquad (2.12a)$$

Equations (2.11a and b) may be solved for S_1 and S_2. The contact pressure p is then determined by equation (2.11c). Subsituting for p in equation (2.12a), the expression for the frictional torque takes the form,

$$T_f = \mu r_f \left[2 \cos \beta \frac{m_b r \omega_c^2 \cot \alpha - m_b g}{\cos \beta + \sin\beta \cot\alpha} - (m_s g + kx + f_o)\right] \qquad (2.12b)$$

where

$$\sin \alpha = r/\ell$$

$$\cos \beta = \sqrt{\ell^2 - (r - e)^2}/\ell \quad \text{and}$$

$$x = \sqrt{\ell^2 - r_b^2} + \sqrt{\ell^2 - (r_b - e)^2} - \sqrt{\ell^2 - r^2} - \sqrt{\ell^2 - (r-e)^2} \qquad (2.13)$$

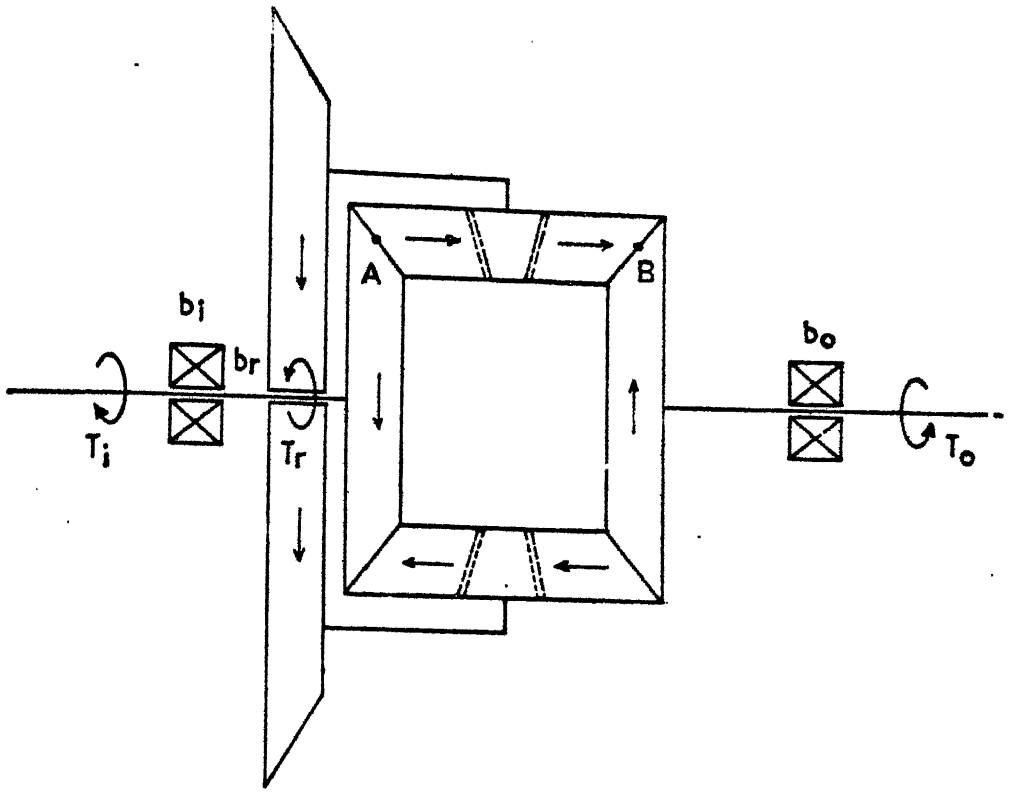

FIG. 2.3 SCHEMATIC DIAGRAM OF THE DIFFERENTIAL GEAR UNIT.

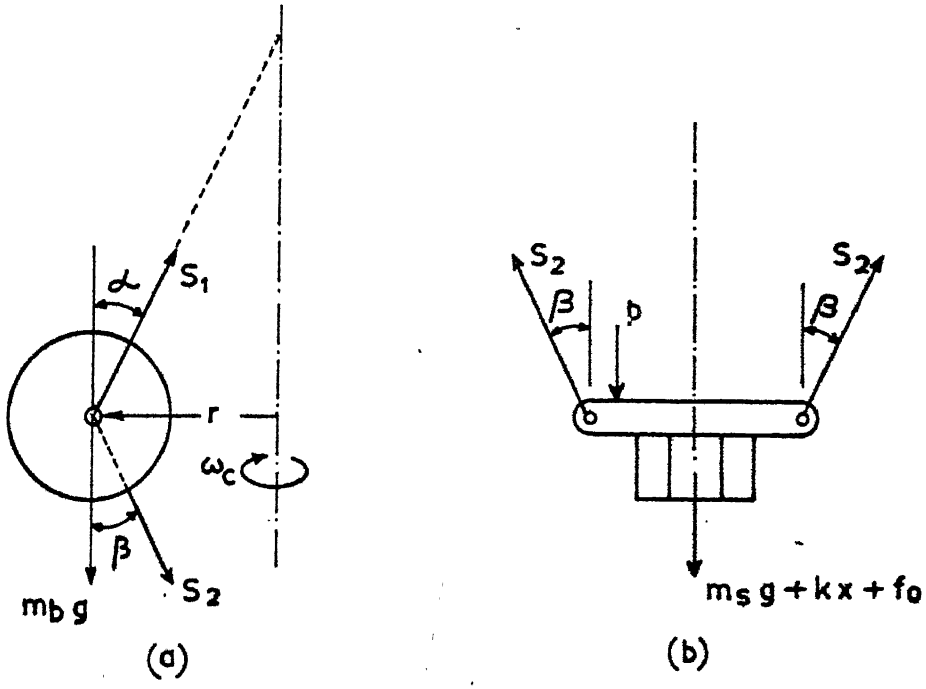

FIG. 2.4 FREE BODY DIAGRAMS OF (a) GOVERNOR BALL (b) GOVERNOR SLEEVE

At steady state, the torque available at the controlling device would be,

$$T_c = T_f + b_c \omega_c \quad . \qquad (2.14)$$

Substituting for T_f in equation (2.14) and using the relation (2.5), the output speed ω_o may be expressed as a function of the torque available at the governor shaft T_c and the governor sleeve position x as,

$$\frac{R^2}{4}(\omega_i - \omega_o)^2 + \frac{b_c}{\mu\, r_f\, m_b r \cot\alpha} \cdot \frac{\cos\beta + \sin\beta \cot\alpha}{2\cos\beta} \cdot \frac{R}{2}(\omega_i - \omega_o)$$

$$= \left[\left(\frac{T_c}{\mu\, r_f} + m_s g + kx + f_o\right) \frac{\cos\beta + \sin\beta \cot\alpha}{2\cos\beta} + m_b g\right] \frac{1}{m_b\, r \cot\alpha}$$

(2.15)

where T_c is given by equation (2.10) and r is related to x by equation (2.13).

The influence of the system parameters on the system characteristics was evaluated next. In view of the large number of design parameters, a governor configuration with the following fixed parameter values was considered.

ℓ	= 10 cms	r_f	= 1.5 cms	μ	= 0.3
e	= 2 cms	m_b	= 0.1 kg	ω_i	= $\frac{2\pi \cdot 500}{60}$ rad/sec
r_b	= 2 cms	m_s	= 0.3 kg	$b_i = b_o = b_r = b_c$	= 0.0
f_o	= 50 Newtons	k	= 50 N/cm .		

The governor ball mass m_b, spring stiffness k and the step ratio R were varied over the range of interest.

Fig. 2.5 shows the variation of output speed ω_o with the governor sleeve position x for three different values of the output torque T_o and the step ratio R. The plots, for any value of step ratio R, indicate that (a) the range of speed variation remains nearly the same for all values of the output load torque and (b) the drop in the output speed due to increase in output torque is also nearly the same at all sleeve positions. For high values of R, the curves shift upwards and come closer together. Increasing the step ratio R thus provides the desirable feature of reducing the system sensitivity to output load torque changes. However, it also results in a reduction of the speed range which the system can provide.

Fig. 2.6 shows the influence of the governor ball mass m_b on the system characteristic for different output load torque T_o. It is observed that the effect of m_b on the system characteristic is similar to that of the step ratio R discussed above. The affect of the governor spring stiffness is indicated in Fig. 2.7. Like R and m_b, increase in k also reduces the system sensitivity to output load changes. In contrast, however, higher stiffness leads to an increased speed range. While increasing the spring stiffness is desirable its maximum value would be limited by the strength of the governor links.

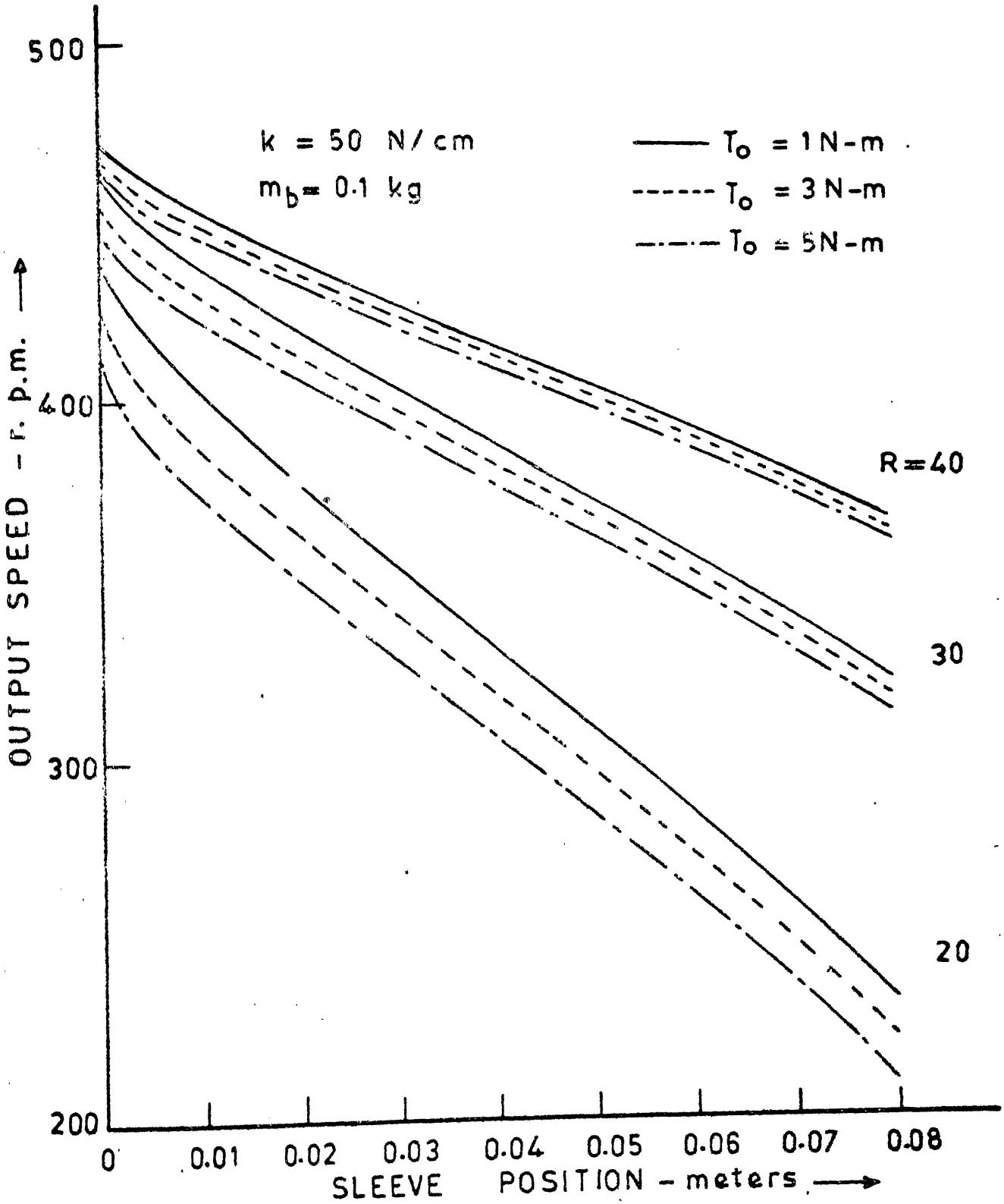

FIG. 2.5 EFFECT OF STEP RATIO R ON THE SYSTEM CHARACTERISTICS

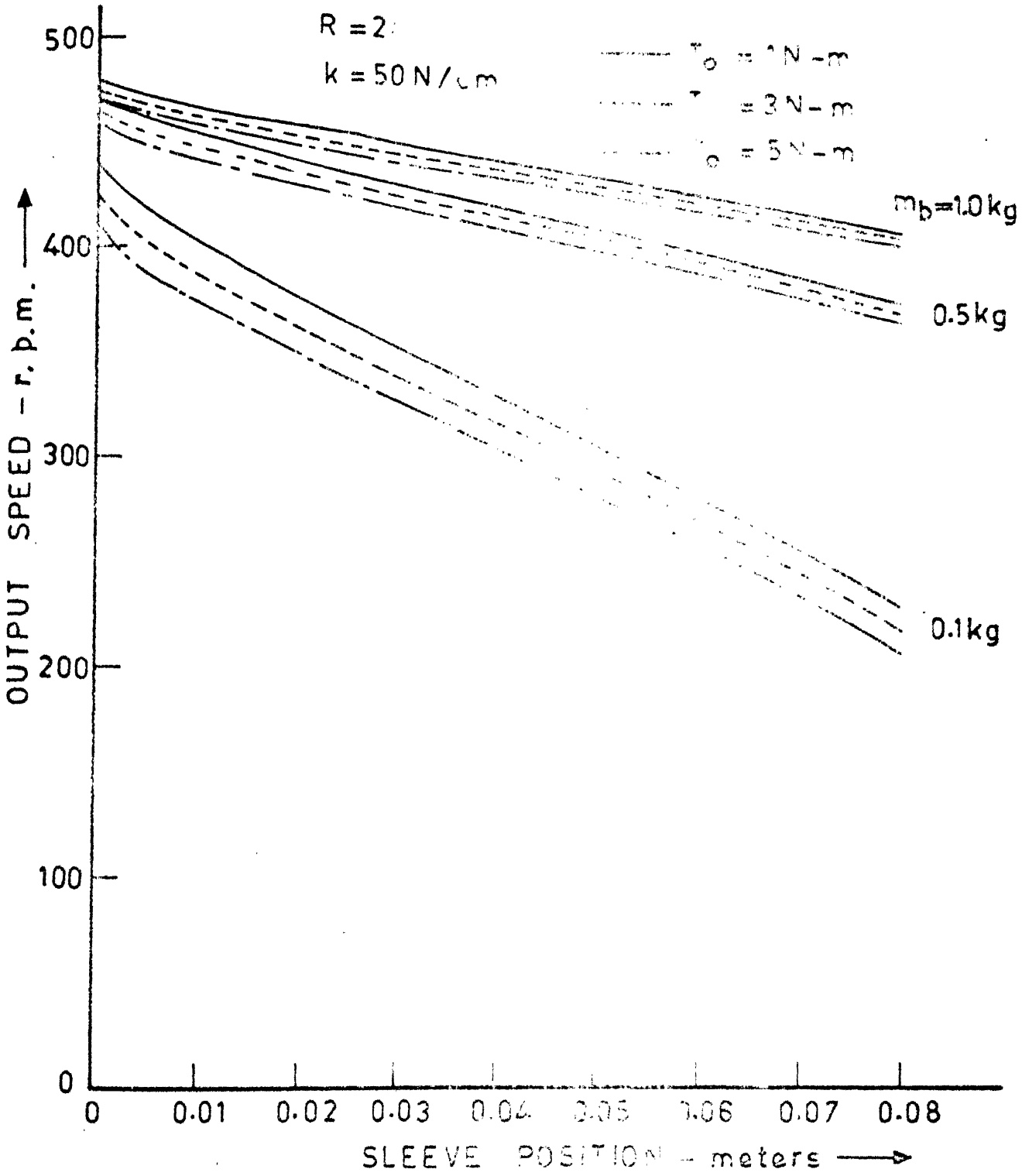

FIG.2.6 EFFECT OF GOVERNOR BALL MASS m_b ON THE SYSTEM CHARACTERISTICS

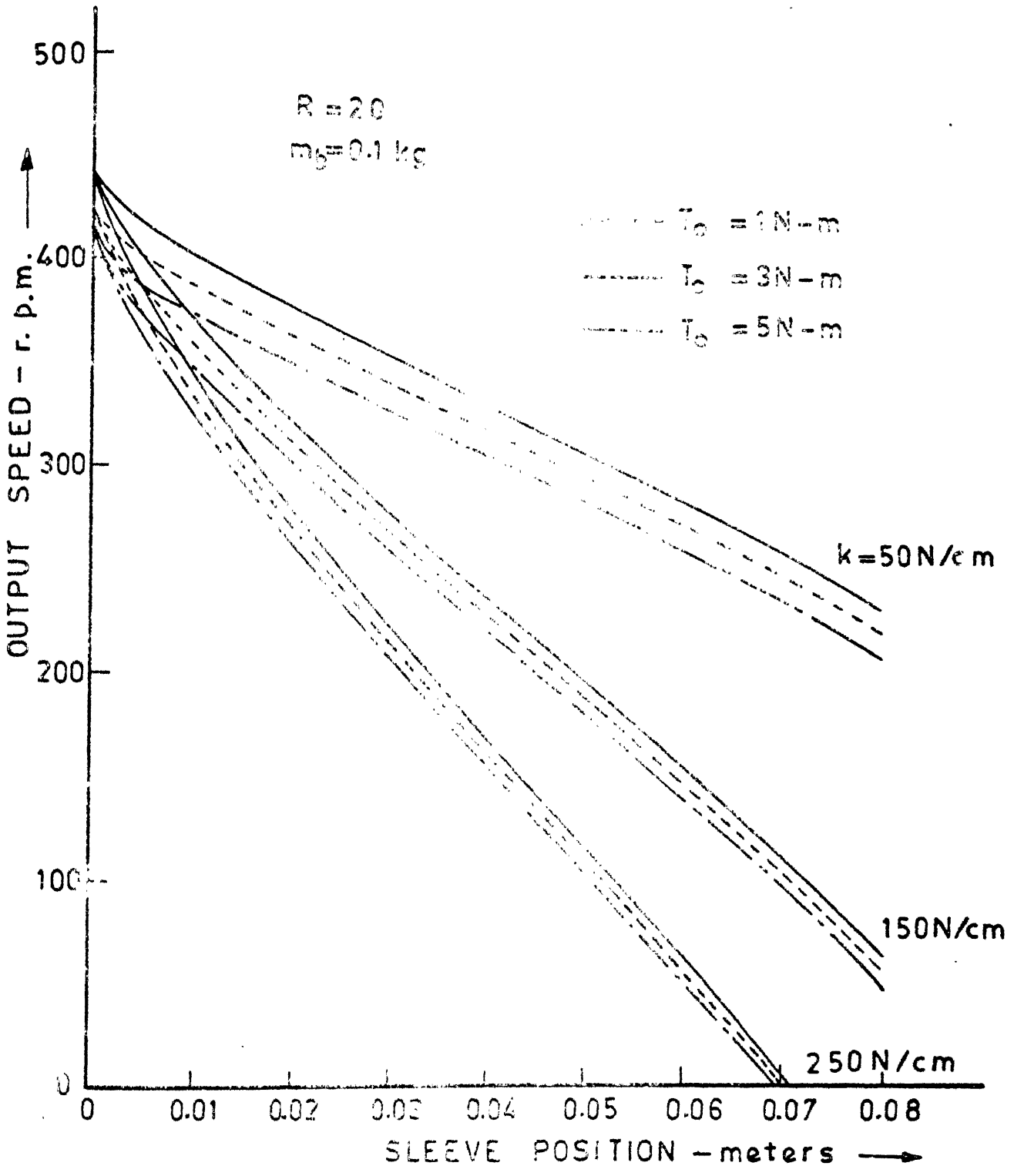

FIG.2.7 EFFECT OF SPRING STIFFNESS k ON THE SYSTEM CHARACTERISTICS.

2.1.2 Dynamic Analysis

It would be of interest to examine the speed of response of the differential gear ball governor system to changes in the governor sleeve position and the output load torque. A dynamic analysis is therefore carried out to study its transient behaviour. The system time constant is derived through a linearized analysis. The transient response predicted by the linear analysis is compared with the results obtained through the solution of the exact non-linear equations.

Fig. 2.8a shows the output shaft and the output bevel gear assembly, indicating the output load torque T_o, the bearing resistance moment $b_o\omega_o$ and the forces exerted by the planets on the output bevel gear. The equation of rotational motion about the input-output axis may be written as,

$$I_o \dot{\omega}_o + b_o\omega_o = (P_{1t} + P_{2t}) r_{po} - T_o . \quad (2.16)$$

Fig. 2.8b shows the three force components and two moment components exerted by each of the planet gear and three force components exerted by the pinion on the planet carrier. The bearing friction torque $b_r\omega_r$ is also indicated. The equation of rotational motion is,

$$I_r \dot{\omega}_r + b_r\omega_r = (R_{1t} + R_{2t}) r_{pi} - Q_t r_{pr} - (M_{R1y} + M_{R2y}) . \quad (2.17)$$

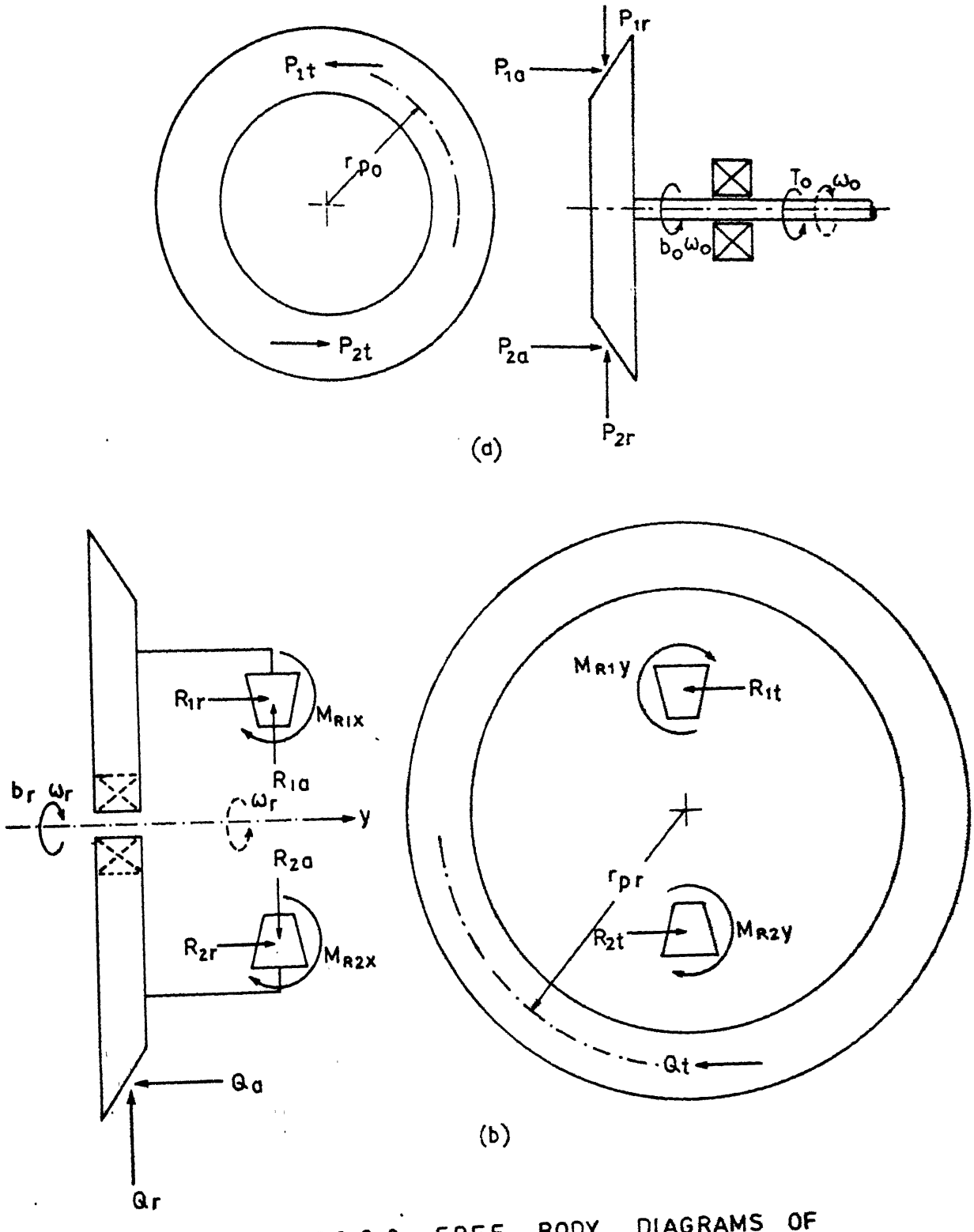

FIG. 2.8 FREE BODY DIAGRAMS OF
(a) OUTPUT SHAFT WITH OUTPUT BEVEL GEAR.
(b) PLANET CARRIER.

The force Q_t results in a moment $Q_t\, r_{pp}$ about the pinion axis which, through the transmission, drives the ball governor against the frictional torque T_f. This driving torque is also opposed by the friction in the bearings supporting the intermediate shafts and the ball governor shaft. Reflecting the various moments of inertia, viscous bearing frictions and the control device frictional torque T_f about the pinion axis, the following equation of motion is obtained,

$$I_{eq}\,\dot{\omega}_r + b_{eq}\,\omega_r = Q_t\, r_{pr} - T_f\, R \qquad (2.18)$$

where

$$\left.\begin{aligned} I_{eq} &= I_1 \left(\frac{r_{pr}}{r_{pp1}}\right)^2 + I_2 \left(\frac{r_{pr}}{r_{pp1}}\right)^2 \left(\frac{r_{pp2}}{r_{pp3}}\right)^2 \\ &\quad + I_c \left(\frac{r_{pr}}{r_{pp1}}\right)^2 \left(\frac{r_{pp2}}{r_{pp3}}\right)^2 \left(\frac{r_{pp4}}{r_{pp5}}\right)^2 \\ b_{eq} &= b_1 \left(\frac{r_{pr}}{r_{pp1}}\right)^2 + b_2 \left(\frac{r_{pr}}{r_{pp1}}\right)^2 \left(\frac{r_{pp2}}{r_{pp3}}\right)^2 \\ &\quad + b_c \left(\frac{r_{pr}}{r_{pp1}}\right)^2 \left(\frac{r_{pp2}}{r_{pp3}}\right)^2 \left(\frac{r_{pp4}}{r_{pp5}}\right)^2 \end{aligned}\right\}. \qquad (2.19)$$

Equations (2.16), (2.17) and (2.18) involve five unknowns, namely, ω_o, $(P_{1t} + P_{2t})$, $(R_{1t} + R_{2t})$, Q_t and

$(M_{R1y} + M_{R2y})$. Thus, two additional relations involving these unknowns are required. To this end, it is necessary to examine the dynamics of the two planet bevel gears.

Fig. 2.9a shows the complete free body diagram of the upper output bevel gear indicating the three force components exerted by the input bevel gear, three force components exerted by the output bevel gear, and three force components and two moment components exerted by the pin. The coordinate system xyz is defined such that the y-axis is aligned with the input-output axis of the system. The z-axis coincides with the geometric axes of the planet gears, which spin relative to it with angular velocity ω_r. The x-axis completes the right-handed triad xyz.

The external force vector acting on the upper planet may be expressed as,

$$\bar{F} = (N_{1t} + P_{1t} - R_{1t})\,\bar{i} + (N_{1a} - P_{1a} - R_{1r})\,\bar{j} + (N_{1r} + P_{1r} - R_{1a} - m_p\, g)\,\bar{k} \quad . \qquad (2.20)$$

The equation of motion for the centre of mass of the upper planet bevel gear then becomes,

$$\bar{F} = r_{pi}\,\dot{\omega}_r\,\bar{i} - r_{pi}\,\omega_r^2\,\bar{k} \quad . \qquad (2.21)$$

The external moment acting about O is given by,

$$\bar{M} = [(P_{lr} - N_{lr})\, r_{pp} + (P_{la} + R_{lr} - N_{la})\, r_{pi} + M_{Rlx}]\, \bar{i}$$

$$+ [(N_{lt} + P_{lt} - R_{lt})\, r_{pi} + M_{Rly}]\, \bar{j}$$

$$+ (N_{lt} - P_{lt})\, r_{pp}\, \bar{k} \quad . \qquad (2.22)$$

The angular velocities of the xyz reference frame and the upper planet bevel gear are,

$$\bar{\omega}_{xyz} = \omega_r\, \bar{j} \qquad (2.23)$$

$$\bar{\omega} = \omega_r\, \bar{j} + \omega_p\, \bar{k} \quad . \qquad (2.24)$$

The angular momentum of the upper planet gear then becomes,

$$\bar{H} = I_{py}\, \omega_r\, \bar{j} + I_{pz}\, \omega_p\, \bar{k} \qquad (2.25)$$

which leads to the equation of rotational motion,

$$\bar{M} = \left.\frac{d\bar{H}}{dt}\right|_{xyz} + \bar{\omega}_{xyz} \times \bar{H}$$

or

$$\bar{M} = I_{px}\, \omega_r\, \omega_p\, \bar{i} + I_{py}\, \dot{\omega}_r\, \bar{j} + I_{pz}\, \dot{\omega}_p\, \bar{k} \quad . \qquad (2.26)$$

Substituting equations (2.20) in (2.21) and equation (2.22) in equation (2.26), the scalar equations of motion for the upper planet gear are obtained as :

$$N_{1t} + P_{1t} - R_{1t} = m_p\, r_{pi}\, \dot{\omega}_r \qquad (2.27a)$$

$$N_{1a} - P_{1a} - R_{1r} = 0 \qquad (2.27b)$$

$$N_{1r} + P_{1r} - R_{1a} - m_p\, g = -m_p\, r_{pi}\, \omega_r^2 \qquad (2.27c)$$

$$I_{px}\, \omega_r\, \omega_p = (P_{1r} - N_{1r})\, r_{pp} + (P_{1a} + P_{1r} - N_{1a})\, r_{pi} + M_{R1x} \qquad (2.27d)$$

$$I_{py}\, \dot{\omega}_r = (N_{1t} + P_{1t} - R_{1t})\, r_{pi} + M_{R1y} \qquad (2.27e)$$

$$I_{pz}\, \dot{\omega}_p = (N_{1t} - P_{1t})\, r_{pp} \,. \qquad (2.27f)$$

Fig. 2.9b shows the free body diagram of the lower planet bevel gear indicating the force components exerted by the input bevel gear, output bevel gear and the force and moment components exerted by the pin. Following the same approach as for the upper planet gear, the equations of motion for the lower planet bevel gear are found to be,

$$N_{2t} + P_{2t} - R_{2t} = m_p\, r_{pi}\, \dot{\omega}_r \qquad (2.28a)$$

$$N_{2a} - P_{2a} - R_{2r} = 0 \qquad (2.28b)$$

$$N_{2r} + P_{2r} - R_{2r} + m_p g = -m_p r_{pi} \omega_r^2 \qquad (2.28c)$$

$$I_{px} \omega_r \omega_p = (P_{2r} - N_{2r}) r_{pp} + (P_{2a} + R_{2r} - N_{2a}) r_{pi} + M_{R2x} \qquad (2.28d)$$

$$I_{py} \dot{\omega}_r = (N_{2t} + P_{2t} - R_{2t}) r_{pi} + M_{R2y} \qquad (2.28e)$$

$$I_{pz} \dot{\omega}_p = (N_{2t} - P_{2t}) r_{pp} \ . \qquad (2.28f)$$

Solving for M_{R1y} from equations (2.27a) and (2.27e) results in,

$$M_{R1y} = (I_{py} - m_p r_{pi}^2) \dot{\omega}_r \ .$$

Similarly, the expression for M_{R2y} may be obtained from equations (2.28a) and (2.28e) as,

$$M_{R2y} = (I_{py} - m_p r_{pi}^2) \dot{\omega}_r \ .$$

Adding the above two equations results in,

$$M_{R1y} + M_{R2y} = 2 (I_{py} - m_p r_{pi}^2) \dot{\omega}_r \ . \qquad (2.29)$$

Adding equations (2.27a) and (2.27f) after substituting for $\dot{\omega}_p$ from equation (2.1) results in,

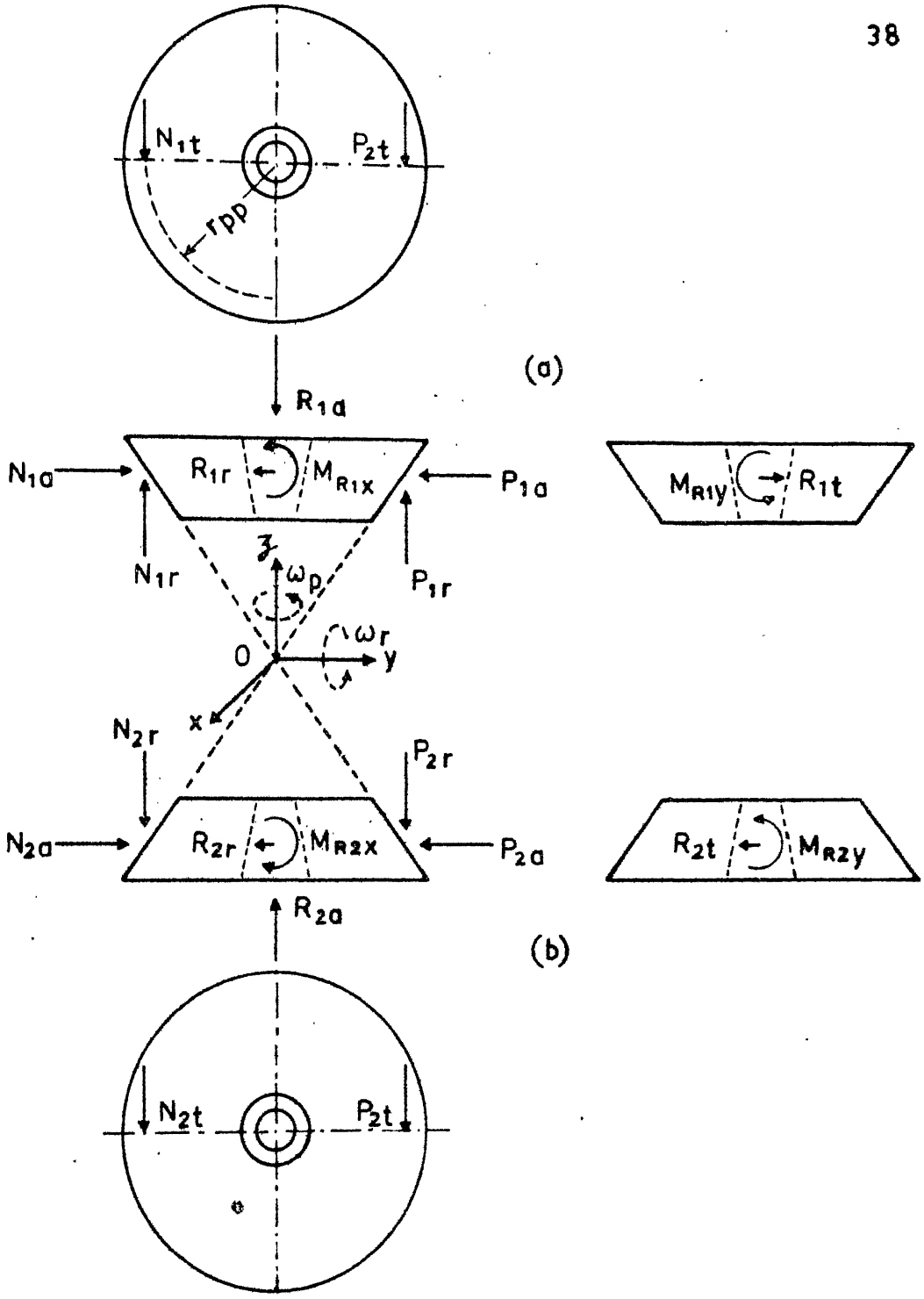

FIG. 2.9 FREE BODY DIAGRAMS OF
(a) UPPER PLANET GEAR.
(b) LOWER PLANET GEAR.

$$2\,N_{1t} - R_{1t} = \left(m_p\, r_{pi} - I_{pz}\,\frac{r_{po}}{r_{pp}^{\,2}}\right)\dot{\omega}_r \,.$$

Similarly, from equations (2.28a) and (2.28f) the following expression may be obtained,

$$2\,N_{2t} - R_{2t} = \left(m_p\, r_{pi} - I_{pz}\,\frac{r_{po}}{r_{pp}^{\,2}}\right)\dot{\omega}_r \,.$$

Adding the above two expressions results in,

$$2(N_{1t} + N_{2t}) - (R_{1t} + R_{2t}) = 2\left(m_p\, r_{pi} - I_{pz}\,\frac{r_{po}}{r_{pp}^{\,2}}\right)\dot{\omega}_r \,. \qquad (2.30)$$

Adding equations (2.27f) and (2.28f) after substituting for $\dot{\omega}_p$ from equation (2.1), the following expression may be obtained,

$$(N_{1t} + N_{2t}) - (P_{1t} + P_{2t}) = -\,2\,I_{pz}\,\frac{r_{po}}{r_{pp}^{\,2}}\,\dot{\omega}_r \,. \qquad (2.31)$$

Eliminating $(N_{1t} + N_{2t})$ from equations (2.30) and (2.31) results in,

$$2(P_{1t} + P_{2t}) - (R_{1t} + R_{2t}) = \left(2\,m_p\, r_{pi} + 2\,I_{pz}\,\frac{r_{po}}{r_{pp}^{\,2}}\right)\dot{\omega}_r \,. \qquad (2.32)$$

Equations (2.29) and (2.32) represent the relations sought from the dynamics of the planet bevel gears. From equations (2.16), (2.17), (2.18), (2.29) and (2.32), the desired equation governing the output speed ω_o is finally obtained as,

$$\left[I_o + \frac{1}{4} (I_r + 2 I_{py} + I_{eq} + 2 I_{pz} \frac{r_{po}^2}{r_{pp}^2} \right] \dot{\omega}_o$$

$$+ [b_o + \frac{1}{4} (b_r + b_{eq})] \omega_o - \frac{1}{4} (b_r + b_{eq}) \omega_i = \frac{1}{2} T_f R - T_o . \qquad (2.33)$$

Note that T_f given by equation (2.12b) is a non-linear function of the output speed ω_o (through the kinematic relation (2.5)) and the governor sleeve position x. The dynamic behaviour of the system is thus described by a first order non-linear differential equation.

In order to gain some physical insight and to suggest possible improvements to the transient behaviour, an analytical expression for the system time constant is obtained. For this purpose it is necessary to linearize the expression for frictional torque T_f (equation 2.12b). This results in,

$$\Delta T_f = - K_1 \Delta \omega_o - K_2 \Delta x \qquad (2.34)$$

where K_1 and K_2 are positive constants defined as,

$$K_1 = -\frac{\partial T_f}{\partial \omega_o}\bigg|_0 \quad \text{and} \quad K_2 = -\frac{\partial T_f}{\partial x}\bigg|_0 ,$$

the partial derivatives being evaluated at the operating condition. After considerable algebra, these may be expressed as,

$$K_1 = \mu\, r_f\, m_b\, R^2\, (\omega_o - \omega_i)\, \frac{r\sqrt{\ell^2 - r^2}\,\sqrt{\ell^2 - (r-e)^2}}{r\sqrt{\ell^2 - (r-e)^2} + (r-e)\sqrt{\ell^2 - r^2}}\bigg|_0 \tag{2.35}$$

and

$$K_2 = \mu\, r_f \{ m_b(\omega_i - \omega_o)^2 \frac{R^2}{2} \sqrt{\ell^2 - r^2}\,\sqrt{\ell^2 - (r-e)^2}\, \{ [r\sqrt{\ell^2-(r-e)^2}$$

$$+ (r-e)\sqrt{\ell^2 - r^2}]\, [\sqrt{\ell^2-(r-e)^2}\,\sqrt{\ell^2 - r^2}$$

$$+ r\,(\frac{2r^3 - 3r^2e - 2r\ell + re^2 + e\ell^2}{\sqrt{\ell^2 - r^2}\,\sqrt{\ell^2 - (r-e)^2}})]$$

$$- r\sqrt{\ell^2-(r-e)^2}\,\sqrt{\ell^2 - r^2}\,[\sqrt{\ell^2-(r-e)^2} + \sqrt{(\ell^2 - r^2)}$$

$$- \frac{r(r-e)}{\sqrt{\ell^2-(r-e)^2}} - \frac{r(r-e)}{\sqrt{\ell^2 - r^2}}]\} \,/\, [r\sqrt{\ell^2-(r-e)^2} + (r-e)\sqrt{(\ell^2-r^2)}]^3]$$

$$- 2\, m_b\, g\, \sqrt{\ell^2-r^2}\,\sqrt{\ell^2-(r-e)^2}\, \{[r\sqrt{\ell^2-(r-e)^2} + (r-e)\sqrt{\ell^2-r^2}]$$

$$[\sqrt{\ell^2-(r-e)^2} - \frac{r(r-e)}{\sqrt{\ell^2-(r-e)^2}}] - r\sqrt{\ell^2-(r-e)^2}\,[\sqrt{\ell^2-(r-e)^2}$$

$$+ \sqrt{\ell^2 - r^2} - \frac{r(r - e)}{\sqrt{\ell^2 - (r - e)^2}} - \frac{r(r - e)}{\sqrt{\ell^2 - r^2}} \Big] \Big\} \Big/ \Big[r\sqrt{\ell^2 - (r - e)^2}$$

$$+ (r - e)\sqrt{\ell^2 - r^2} \Big]^3 - k \Big\} \Big|_0 \quad . \tag{2.36}$$

The linearized system equation then becomes,

$$C_1 \Delta\dot{\omega}_o + C_2 \Delta\omega_o = - C_3 \Delta x - \Delta T_o \tag{2.37}$$

where

$$\left.\begin{aligned} C_1 &= I_o + \tfrac{1}{4} (I_r + 2 I_{py} + 2 I_{pz} r_{po}/r_{pp}^2 + I_{eq}) \\ C_2 &= b_o + \tfrac{1}{4} (b_r + 2 K_1 R + b_{eq}) \\ C_3 &= \tfrac{1}{2} R K_2 \quad . \end{aligned}\right\} \tag{2.38}$$

The system time constant is given by,

$$\tau = \frac{I_o + \frac{1}{4} (I_r + 2 I_{py} + 2 I_{pz} r_{po}^2/r_{pp}^2 + I_{eq})}{b_o + \frac{1}{4} (b_r + K_1 R + b_{eq})} \quad . \tag{2.39}$$

It appears interesting to study the dependence of the system time constant on the design parameters. The number of parameters being large, only the effect of the governor ball mass m_b is studied presently. Equation (2.39) shows that m_b influences the time constant through the terms I_{eq} and K_1.

Explicit dependence of I_{eq} on m_b is given by ,

$$I_{eq} = I_1 \left(\frac{r_{pr}}{r_{pp1}}\right)^2 + I_2 \left(\frac{r_{pr}}{r_{pp1}}\right)^2 \left(\frac{r_{pp2}}{r_{pp3}}\right)^2 + [I + 2m_b (\tfrac{2}{5} r_b^2 + r^2)]R^2. \tag{2.40}$$

The dependence of K_1 on m_b is more complicated. An examination of equation (2.35) shows that m_b effects K_1 explicitly, as well as through the quantity $\omega_o|_0$ as,

$$\omega_o\Big|_0 = \omega_i - \sqrt{\frac{C_4}{m_b} + C_5} \tag{2.41}$$

where

$$C_4 = \frac{4}{R^2}\left[\frac{2\,T_o}{\mu\, R\, r_f} + m_s\, g + kx + f_o\right]\left[\frac{r\sqrt{\ell^2-(r-e)^2} + (r-e)\sqrt{\ell^2-r^2}}{2r\sqrt{\ell^2-(r-e)^2}\sqrt{\ell^2-r^2}}\right]\Bigg|_0$$

$$C_5 = \frac{4\,g}{R^2\sqrt{\ell^2-r^2}}\Bigg|_0 .$$

Thus, the time constant τ as an explicit function of the governor ball mass m_b is obtained as,

$$\tau = \frac{C_7 + C_8\, m_b}{C_9 + C_6\sqrt{C_4\, m_b + C_5\, m_b^2}} \tag{2.42}$$

where

$$C_6 = -\frac{\mu\, r_f\, R^3}{4}\,\frac{r\sqrt{\ell^2-r^2}\,\sqrt{\ell^2-(r-e)^2}}{r\sqrt{\ell^2-(r-e)^2} + (r-e)\sqrt{\ell^2-r^2}}\Bigg|_0$$

$$C_7 = I_o + \frac{1}{4}\left(I_r + 2 I_{py} + 2 I_{pz}\, r_{po}^2/r_{pp}^2 + I_1 \left(\frac{r_{pr}}{r_{pp1}}\right)^2 + I_2 \left(\frac{r_{pr}}{r_{pp1}}\right)^2 \left(\frac{r_{pp2}}{r_{pp3}}\right)^2 + I R^2\right)$$

$$C_8 = \frac{1}{2}\left(\frac{2}{5} r_b^2 + r^2\right) R^2 \Big|_0$$

$$C_9 = b_o + \frac{1}{4}\left(b_r + b_{eq}\right).$$

The time constant depends on the operating point determined by the output torque T_o and the sleeve position x in addition to the design parameters like m_b. Fig. 2.10 shows the variation of τ with m_b for various values of output load torque T_o. The flat nature of the curves indicate that a low time constant may be obtained over a range of values of the governor ball mass m_b. With increasing output loads the the time constant decreases somewhat. The effect of the sleeve position on the system time constant is presented in Fig. 2.11. The curves clearly indicate the existence of an optimum m_b minimizing the time constant. The optimum value of m_b is found to increase for lower sleeve positions. However, it may still be possible to select a good value of m_b leading to an improved time constant for the entire range of sleeve positions.

Solution of the governing linear differential equation of motion (2.37) for unit step change in sleeve position is,

$$\Delta\omega_o(t) = -\frac{C_3}{C_2}\left(1 - e^{-t/\tau}\right) \qquad (2.43)$$

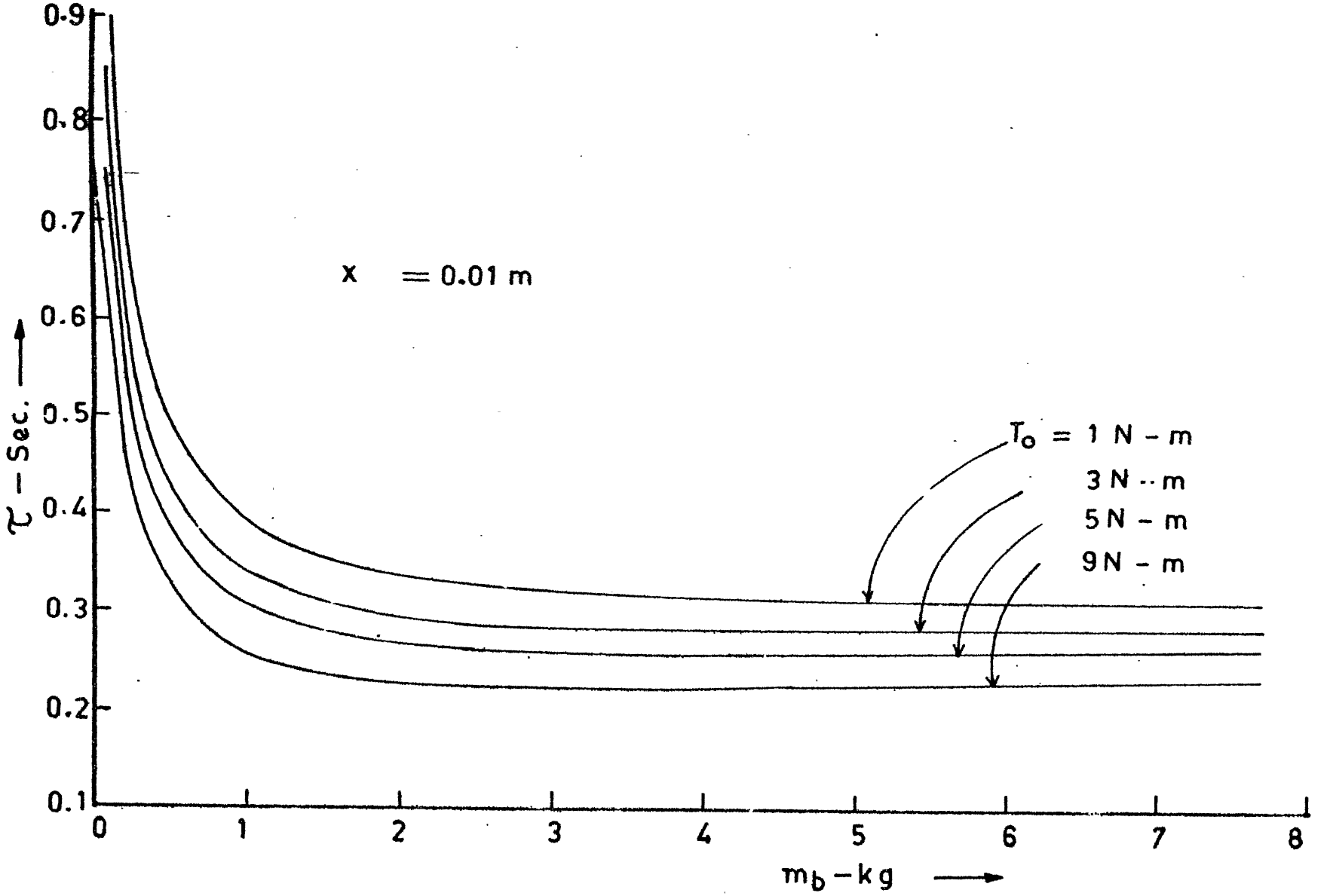

FIG.2.10 VARIATION OF SYSTEM TIME CONSTANT WITH GOVERNOR BALL MASS FOR DIFFERENT OUTPUT LOADS.

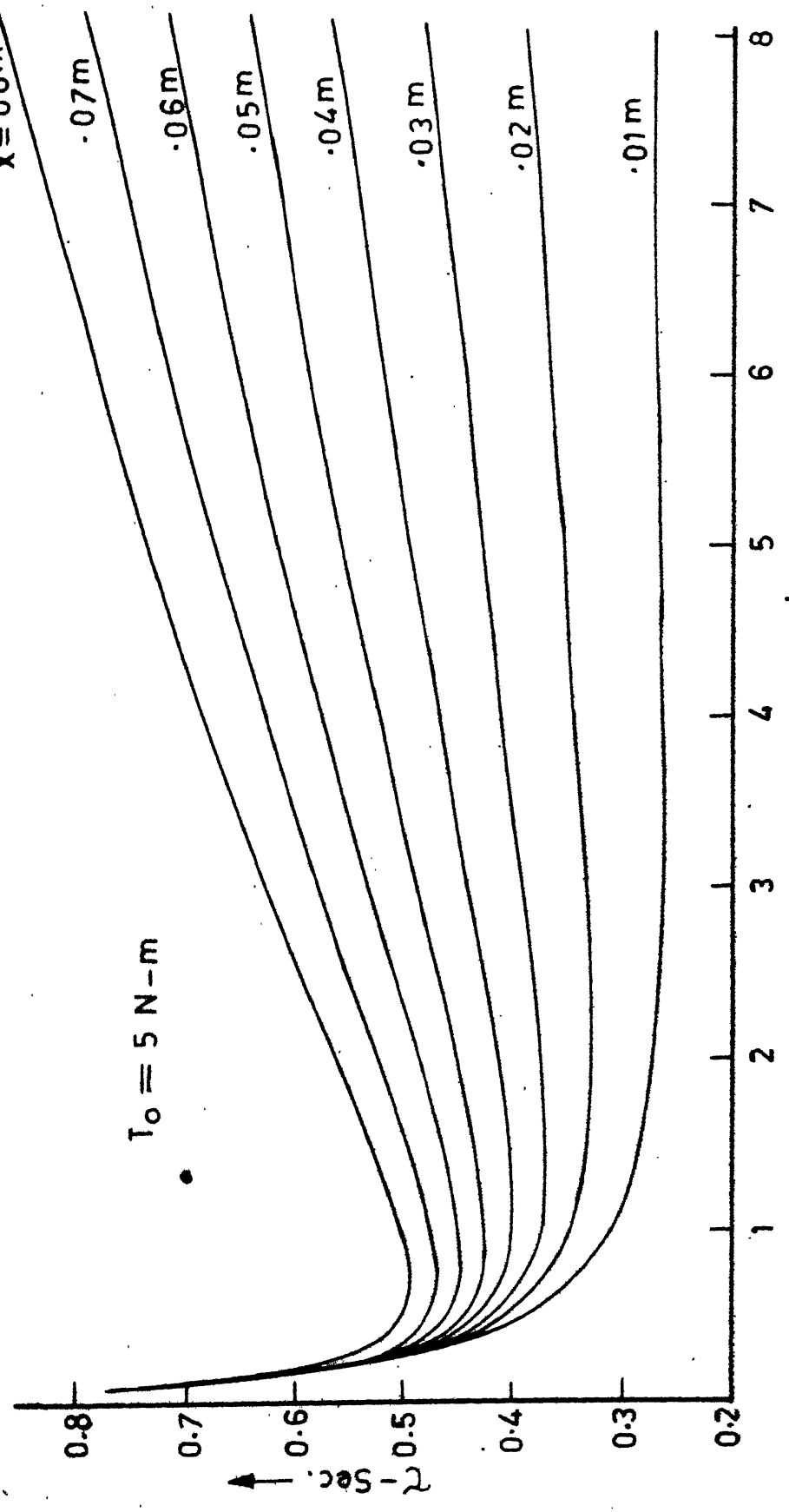

FIG.2.11 VARIATION OF SYSTEM TIME CONSTANT WITH GOVERNOR BALL MASS FOR DIFFERENT SLEEVE POSITIONS.

and for unit step change in output load is,

$$\Delta\omega_o(t) = -\frac{1}{C_2}\left(1 - e^{-t/\tau}\right) . \qquad (2.44)$$

The validity of the linearized analysis was examined by comparing the responses (2.43) and (2.44) with those obtained by integrating the governing non-linear equation of motion (equation 2.33). The following parameter values were assumed for the solution :

$$I_i = I_o = I_r = I_1 = I_2 = I = 0.01 \text{ kg-m}^2 .$$

$$b_i = b_o = b_r = b_1 = b_2 = b_c = 0.0 .$$

$$\frac{r_{pr}}{r_{pp1}} = 1.0 \; ; \; \frac{r_{pp2}}{r_{pp3}} = 4.0 \; ; \; \frac{r_{pp4}}{r_{pp5}} = 5.0 .$$

$$r_{pi} = r_{po} = r_{pp} = 0.03 \text{ m.}$$

$$m_p = 0.3 \text{ kg.}$$

Fig. 2.12 shows the system response to various step changes in sleeve position from an initial operating condition defined by $x = 0.003$ m and $T_o = 5$ N-m. The linear response calculation requires the evaluation of the system time constant. For small step changes in the sleeve position, it may be computed at the initial operating condition. Presently, however, large step changes in the sleeve position are considered. Since the time constant shows a significant variation with the sleeve

position, it was evaluated at a sleeve position representing the mid point of the step maneuver to improve the response prediction. The figure shows the output speed response when the sleeve position is suddenly changed to x = 0.013 m (curve b), x = 0.043m(curve c) and x = 0.083m(curve d) from the initial position of x = 0.003 m (curve a). The plots exhibit excellent agreement between the linear prediction and the exact response for relatively smaller sleeve inputs. Even for very large inputs, the time to reach the new steady state is predicted quite well by the linear response although the steady state error inccreases. The system response to step changes in the output load were obtained similarly by using the time constant evaluated at the mid position of the step change in load. The responses to various step load changes are shown in Fig. 2.13. The above results suggest that the transient response is well predicted by the analytical approach even for quite large percentage changes in the sleeve position and the output load torque.

2.2 DIFFERENTIAL GEAR-PADDLE SYSTEM

In this system, the control output from the differential is connected to a control device consisting of a paddle operating in a liquid container (Fig. 2.14). The liquid tank is provided with baffles which may be rotated to vary the effective baffle width B_W. The power consumption in such a system has been investigated by Costich, Ruston and Everett [6,7]

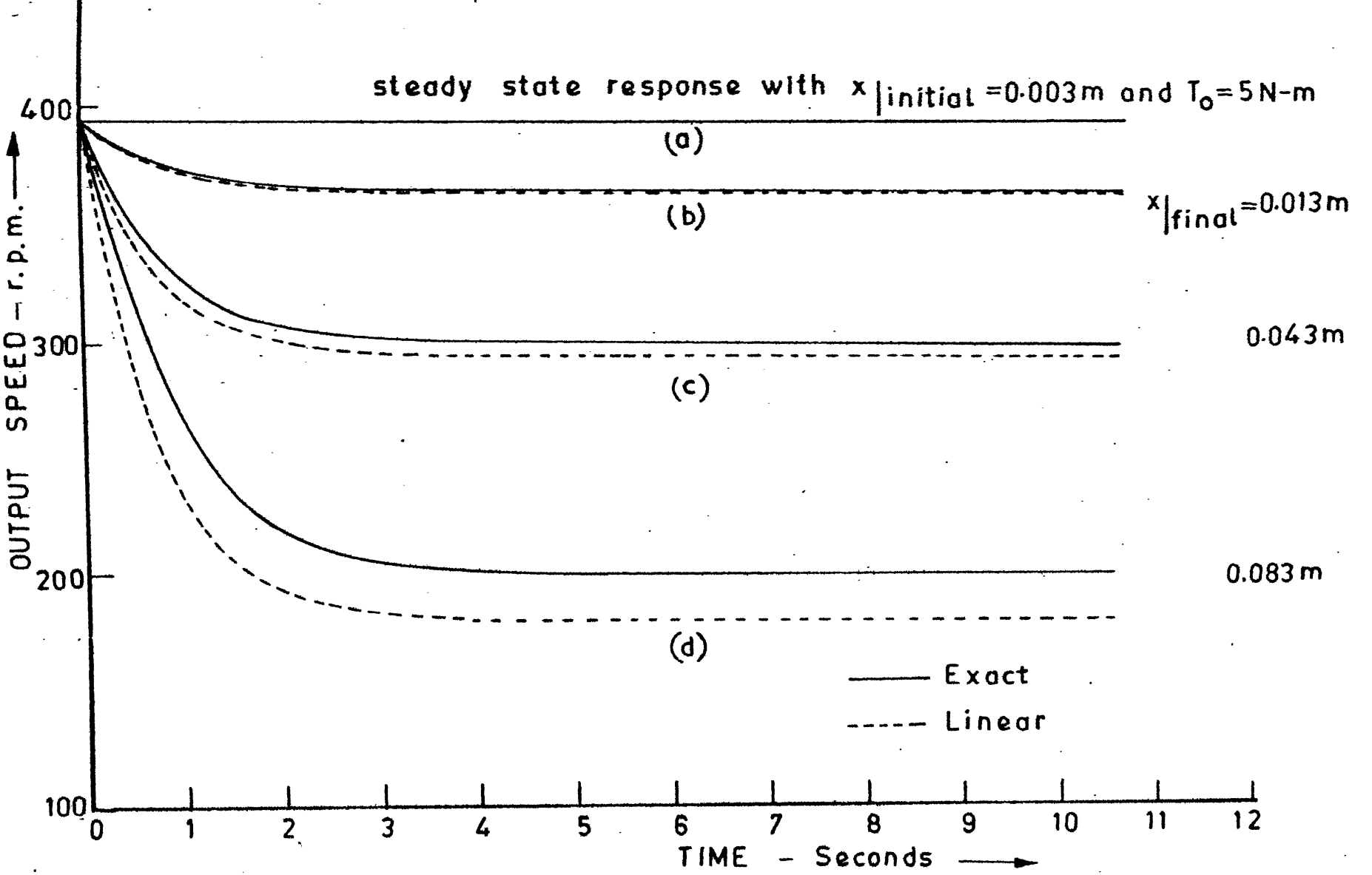

FIG. 2.12 SYSTEM RESPONSE TO STEP CHANGE IN SLEEVE POSITION

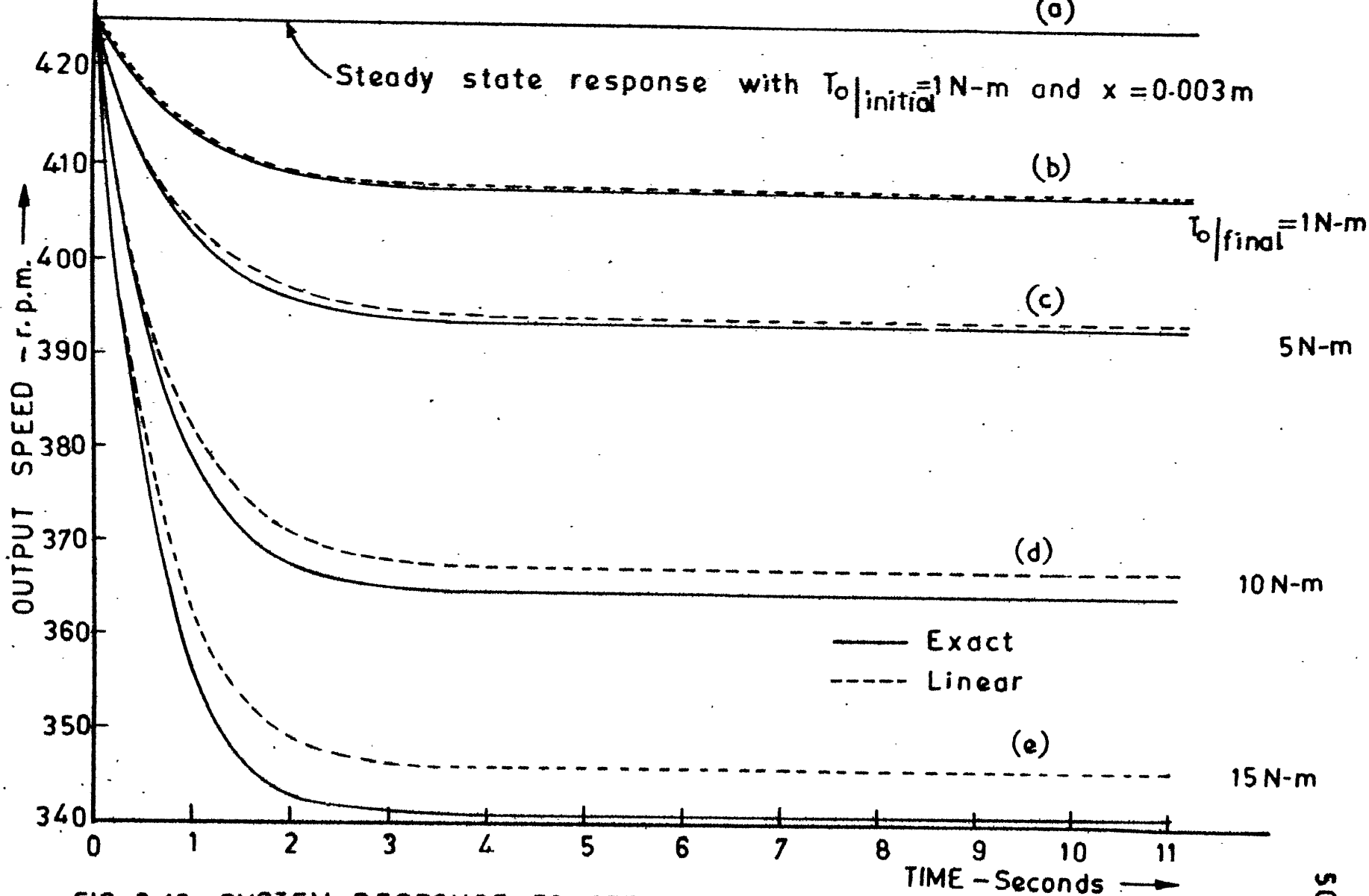

FIG. 2.13 SYSTEM RESPONSE TO STEP CHANGE IN OUTPUT LOAD.

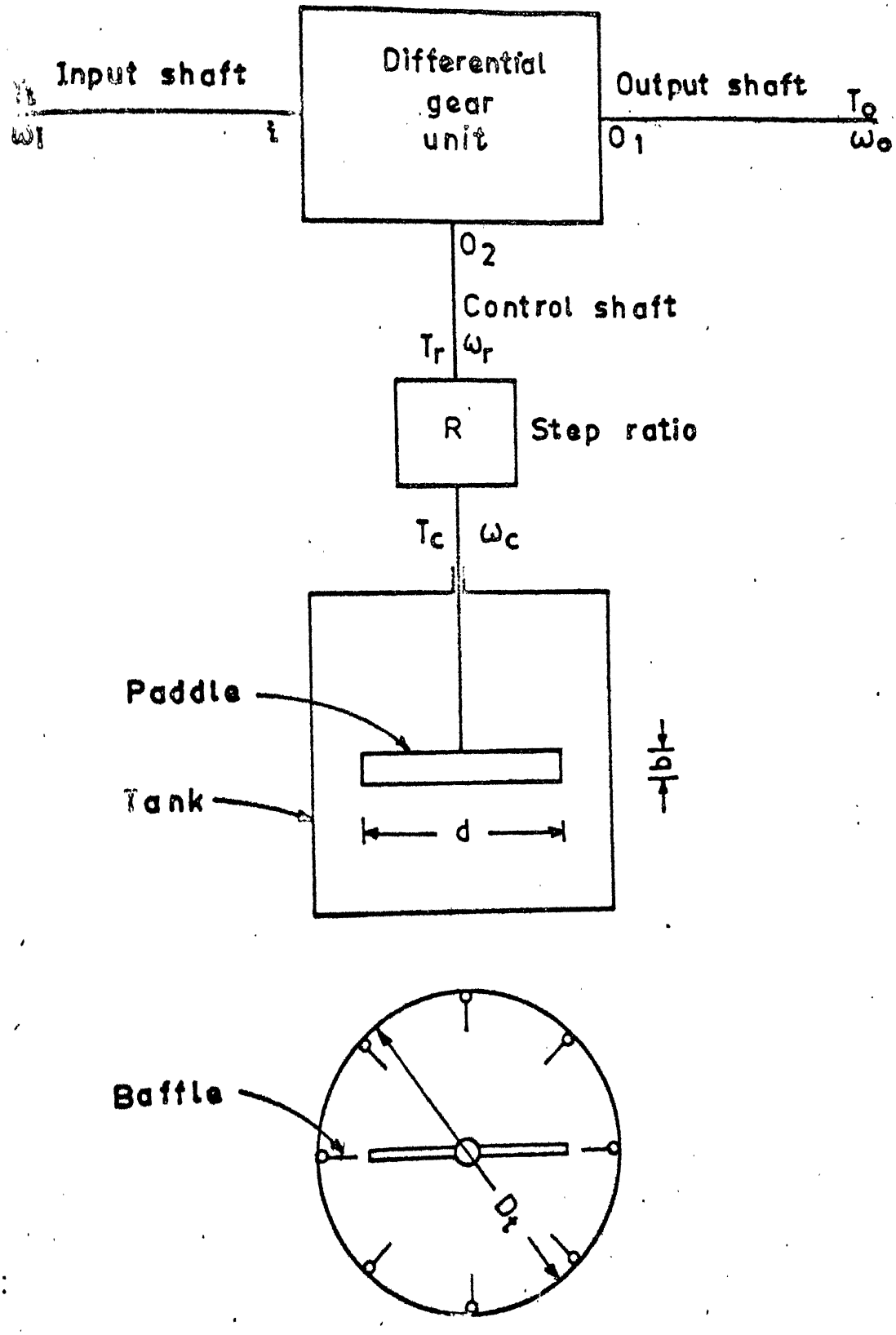

FIG. 2.14 SCHEMATIC DIAGRAM OF THE DIFFERENTIAL GEAR–PADDLE SYSTEM.

and Nagata [8]. These analyses involve the concept of power number defined as,

$$N_p = \frac{\rho D_t^5 \omega_c^3}{P} \quad . \tag{2.45}$$

Nagata obtained the following relation for the power number under fully baffled condition (corresponding to the condition of maximum power consumption),

$$N_{pmax} = \frac{A}{C_{Re}} + B \left(\frac{h}{D_t} \right)^{(0.35 + b/D_t)} \tag{2.46}$$

where

$$\left.\begin{aligned} A &= 14 + (b/D_t) \left[670 \, (d/D_t - 0.6)^2 + 185 \right] \\ C_{Re} &= \frac{25}{b/D_t} \left(\frac{d}{D_t} - 0.4 \right)^2 + \frac{b/D_t}{0.11 \, (b/D_t) - 0.0048} \\ B &= 10^{\left[1.3 - 4 \, (b/D_t - 0.5)^2 - 1.14 \, d/D_t \right]} \end{aligned}\right\} \tag{2.47}$$

The power number under any other baffled condition is obtained from :

$$\frac{N_{pmax} - N_p}{N_{pmax} - N_{p\infty}} = \left[1 - 2.9 \, (B/D_t)^{1.2} \, n \right]^2 \tag{2.48}$$

where

n = number of baffles

$$N_{p\infty} = B\,(0.6/1.6)^{m}$$

with $m = 1.1 + 4\,(b/D_t) - 2.5\,(d/D_t - 0.5)^5 - 7\,(b/D_t)^4$.

Note that the power consumption must be,

$$P = T_c\,\omega_c = \frac{T_o}{R}\,(\omega_i - \omega_o) \quad . \qquad (2.49)$$

Substituting equation (2.49) in equation (2.45) we get,

$$N_p = \frac{\rho\, D_t^{5}\,(\omega_i - \omega_o)^2\, R}{8\, T_o} \quad . \qquad (2.50)$$

Elimination of N_p between equations (2.48) and (2.50) would lead to,

$$\omega_o = \omega_o\,(T_o, B_w)$$

which represents the system steady state characteristic.

The effect of the parameters h, R, b/D_t and d/D_t on the steady state system characteristics was studied. It was found that the ratio of the height of the liquid column to the tank diameter, h/D_t, had little effect on the behaviour.

Fig. 2.15 shows the variation of ω_o with B_w for various step ratios R. The speed range appears to first increase and then decrease with increasing values of R. Higher values of R lead to $\omega_o - T_o$ characteristics with smaller droop which is desirable (Fig. 2.16).

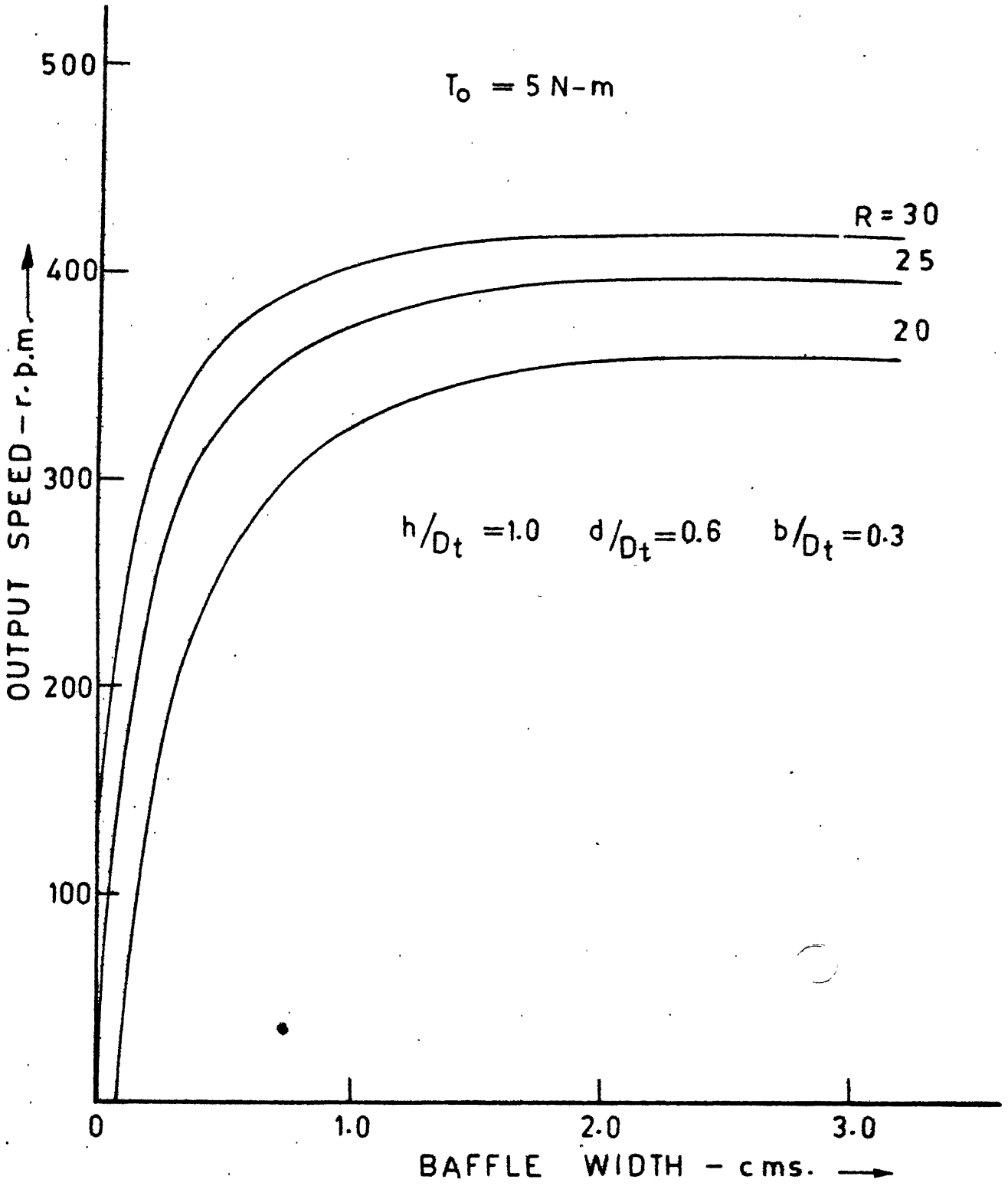

FIG. 2.15 EFFECT OF STEP RATIO R ON THE $\omega_o - B_w$ CHARACTERISTICSOF THE SYSTEM.

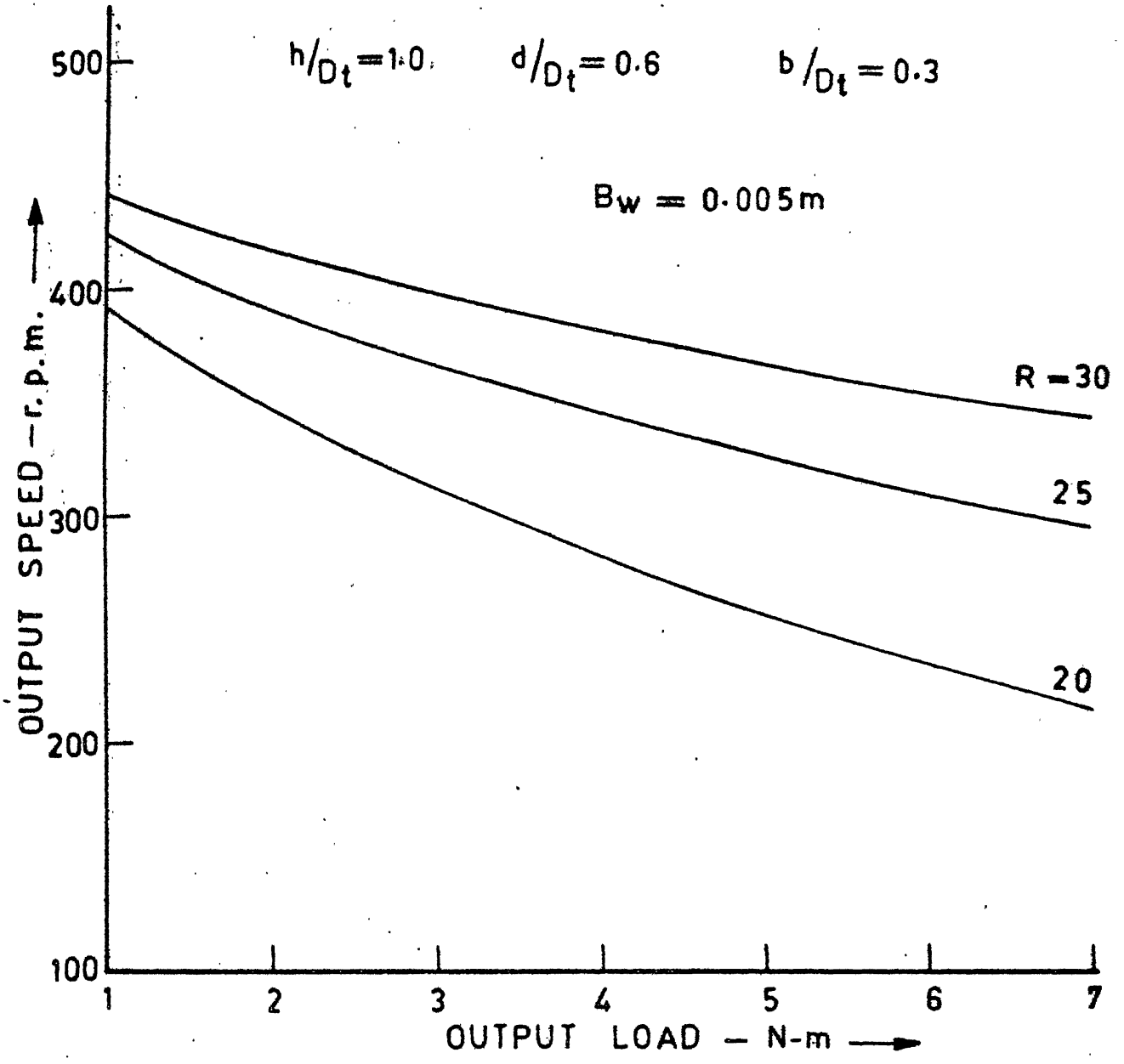

FIG.2.16 EFFECT OF STEP RATIO R ON THE $\omega_o - T_o$ CHARACTERISTICS OF THE SYSTEM.

Fig. 2.17 shows the influence of the parameter d/D_t on the stady state $\omega_o - B_W$ characteristics. The speed range may be increased by increasing d/D_t. Its effect on the variation of output speed with output load is shown in Fig. 2.18. The output speed shows a lower sensitivity to load changes with increasing d/D_t values. The effect of the parameter b/D_t was found to be similar to the affect of d/D_t. The results suggest that the use of a larger impeller leads to increased speed range and lower sensitivity to output load changes.

2.3 DIFFERENTIAL GEAR-DC SHUNT GENERATOR SYSTEM

In this arrangement a d c shunt generator is used as the controlling device. Here the electrical power generated by the machine is dissipated by the load resistance connected in series with the armature. Speed changes are then achieved by varying the load resistance. The steady state analysis of the system is presented below.

Under steady conditions, the equivalent electrical circuit is shown in Fig. 2.19. From the circuit diagram,

$$E = R_a I_a + R_L I_L \tag{2.51}$$

$$I_a = I_f + I_L \tag{2.52}$$

$$I_f = (R_L/R_f) I_L \,. \tag{2.53}$$

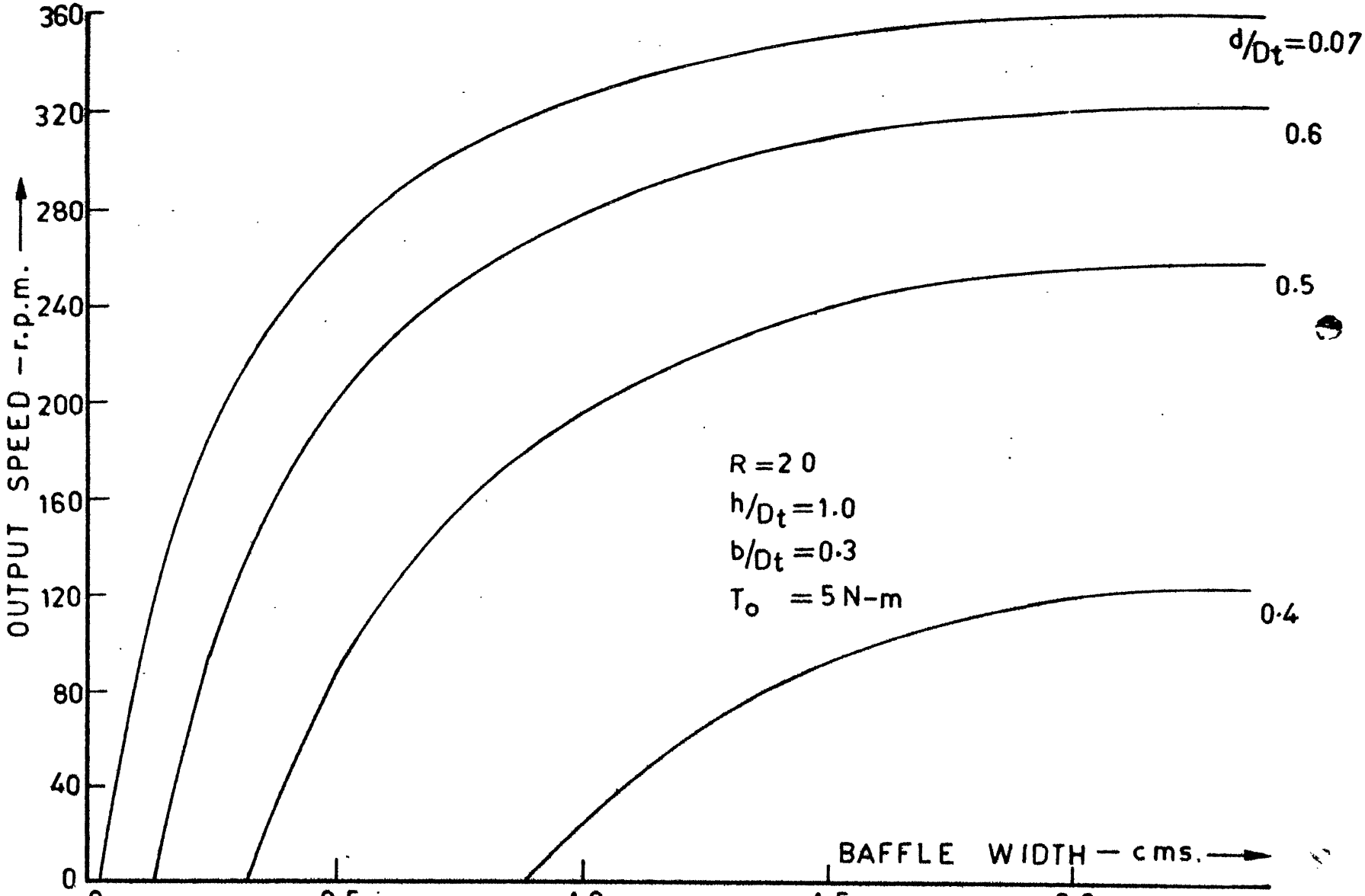

FIG. 2.17 EFFECT OF THE PARAMETER d/D_t ON THE $\omega_o - B_w$ CHARACTERISTICS OF THE SYSTEM.

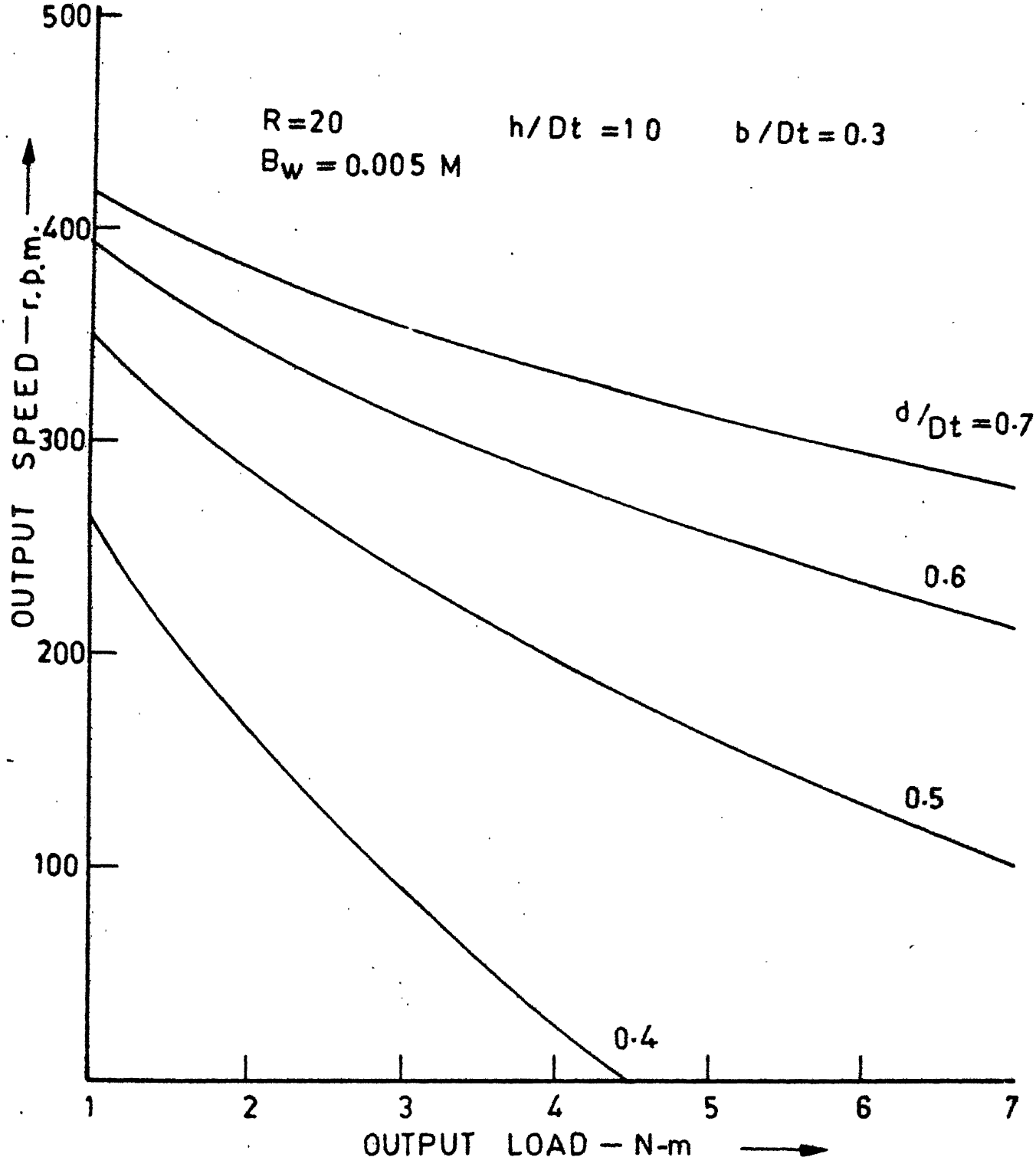

FIG. 2.18 EFFECT OF THE PARAMETER $d/_{Dt}$ ON THE $\omega_o - T_o$ CHARACTERISTICS OF THE SYSTEM.

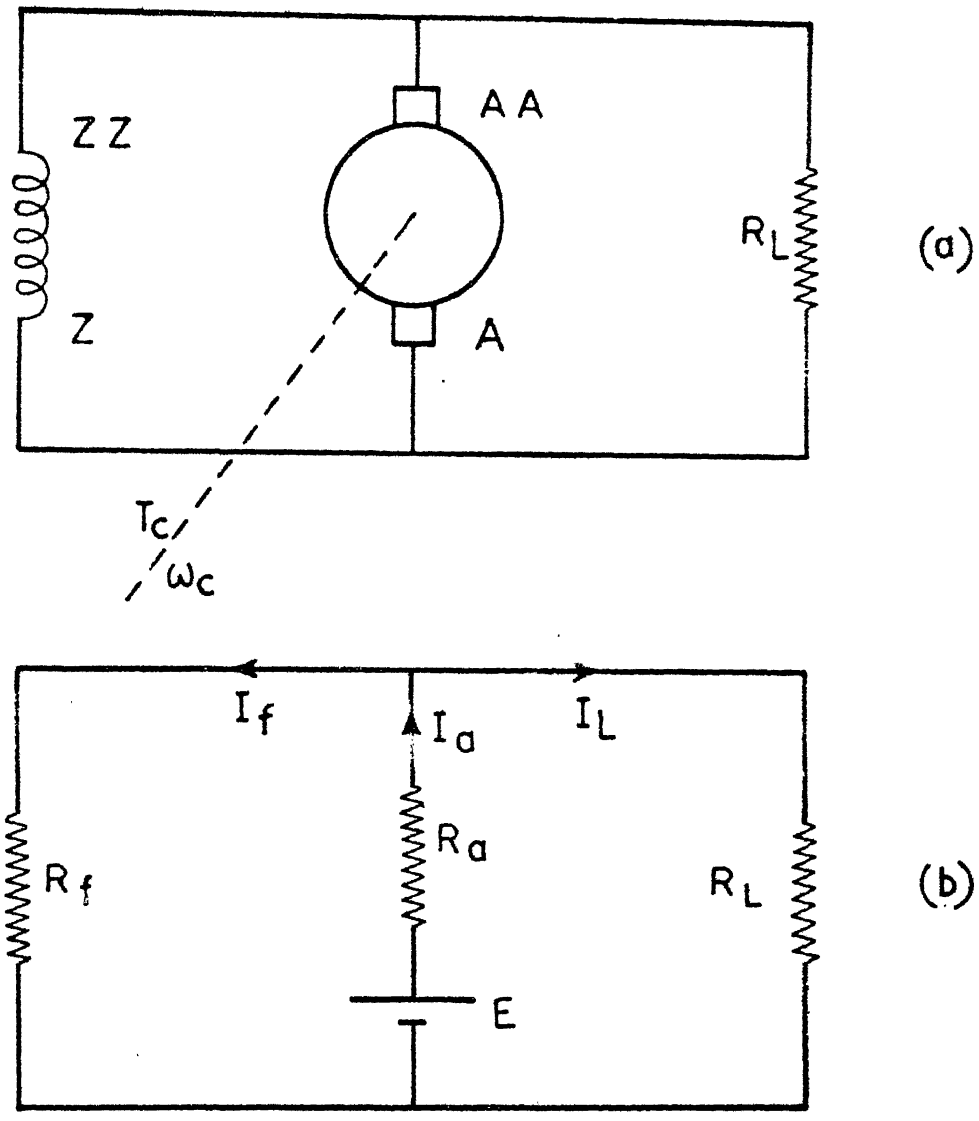

FIG.2.19 EQUIVALENT CIRCUIT DIAGRAM DURING STEADY-STATE OPERATION.

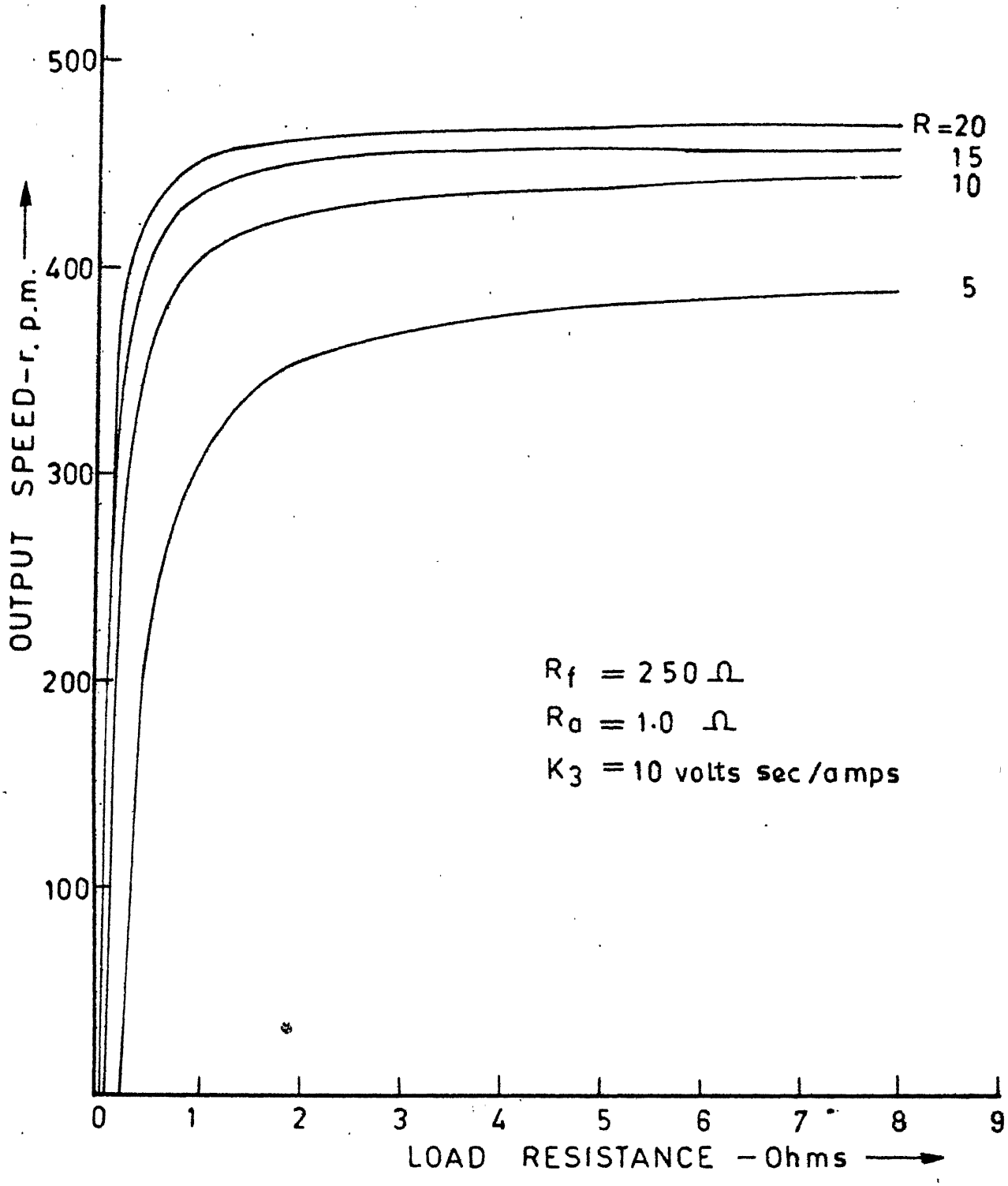

FIG. 2.20 EFFECT OF STEP RATIO R ON THE $\omega_o - R_L$ CHARACTERISTICS OF THE SYSTEM.

CHAPTER 3

EXPERIMENTAL INVESTIGATION

An experiment was carried out to examine the performance of the proposed variable speed drive. A commercially available bevel gear differential (used in three wheeler vehicle) was used in the experimental set-up. The dc shunt generator was chosen as the control device primarly due to the reduced fabrication requirements. The schematic sketch of the system fabricated is shown in Fig. 3.1. A photograph of the experimental set-up appears in Fig. 3.2.

3.1 EXPERIMENTAL SET-UP

A single phase induction motor (0.5 H.P., 1425 rpm) drives the input shaft at 950 rpm through a speed reducing arrangement employing a set of pulleys. The output shaft is loaded by means of a rope-brake dynamometer. The control output speed ω_r from the differential gear is stepped up through the crown wheel (attached to the planet carrier) and pinion combination, and through a set of pulleys, before it is coupled to the dc shunt generator (0.25 H.P., 250 V at 1500 rpm). Provision was made for changing the pulley B in order to carry out the experiment with different values of the step-up ratio R.

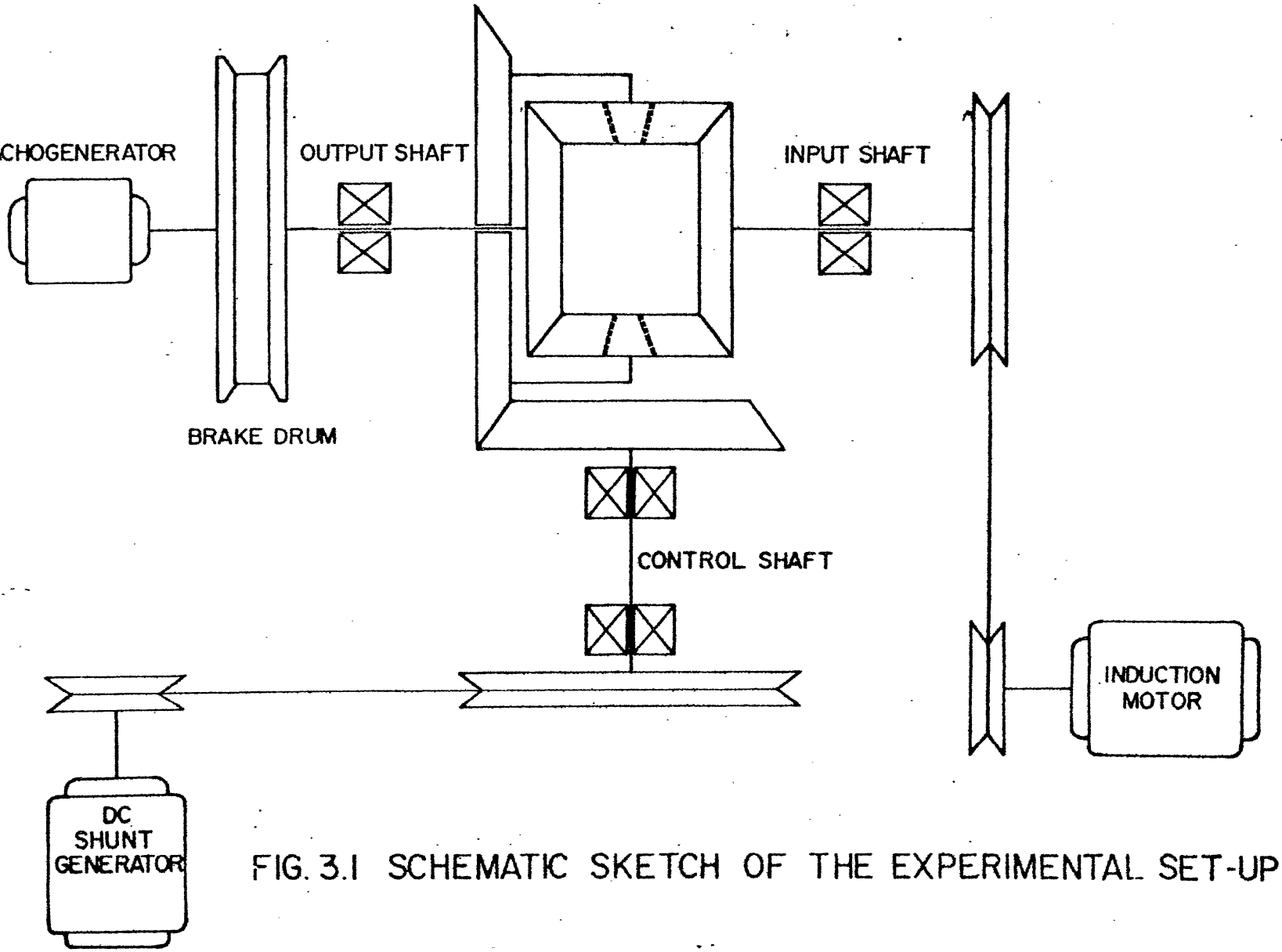

FIG. 3.1 SCHEMATIC SKETCH OF THE EXPERIMENTAL SET-UP

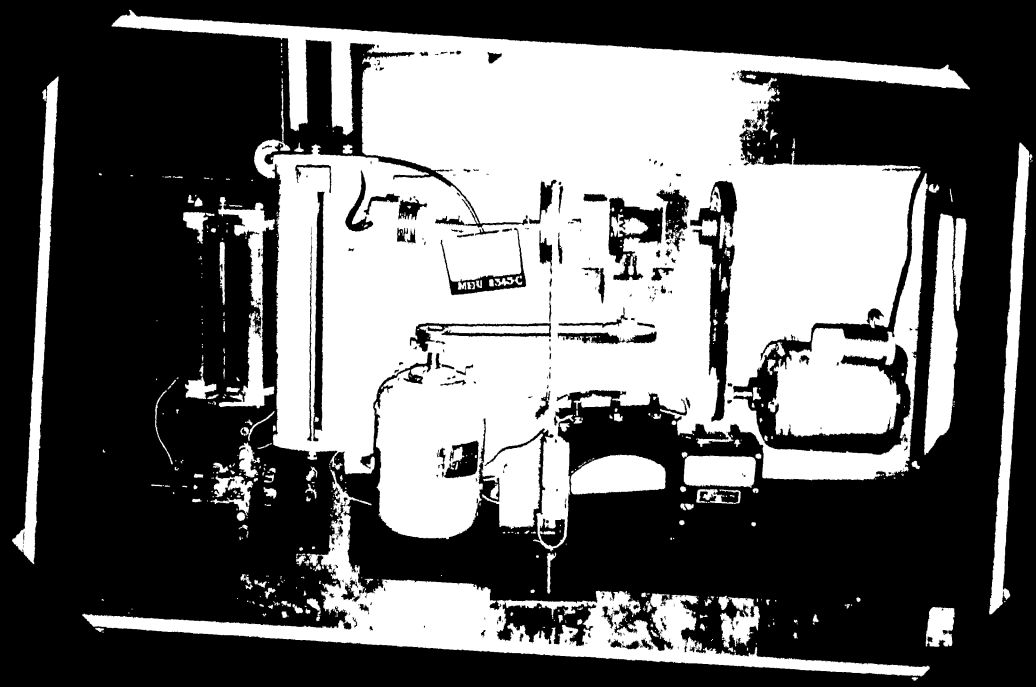

FIG. 3.2 PHOTOGRAPH OF THE EXPERIMENTAL SET-UP

A ac tachogenerator (50 V at 1000 rpm) is coupled to the output shaft to measure the output speed ω_o. A rheostat is used as the load resistance in order to vary the output speeds. A voltmeter and an ammeter are provided in the armature circuit to measure the voltage drop across the load resistance and the load current, respectively.

For a constant load T_o on the output shaft, the output speed ω_o of the system was measured for various values of the load resistance R_L. The ω_o versus R_L characteristic was obtained for different loads T_o on the output shaft. The entire procedure was repeated for three different values of the step ratio R = 3, 4.92 and 6.41.

3.2 RESULTS AND DISCUSSION

The experimentally obtained output speed ω_o versus load resistance R_L characteristics of the differential gear-dc shunt generator system are shown in Fig. 3.3. Curves (a), (b) and (c) show the system characteristic for the step ratio R = 3.0 for three different values of the output load. Each of these curves shows a steep slope with respect to the load resistance for an initial region and then flattens out. For lower range of speeds, large speed variation may be achieved through small changes in the load resistance. In the very high range of speeds, the speed variations which can be achieved become very small. Similar trends are observed for the plots corresponding to R = 4.92 and R = 6.41.

The nature of the $\omega_o - R_L$ characteristics agrees well with the theoretically predicted behaviour.

A comparison of curves (a), (b) and (c) shows the effect of output load T_o on the $\omega_o - R_L$ characteristic. The output speed drops with increase in the output load. Similar feature is observed for the case of R = 4.92 (curves d, e, f) and for R = 6.41 (curves g, h, i). In some cases like curves (h), (i) and curves (e), (f), the speed drop appears to be excessive. The speed change due to output load variations is a feature which was not shown by the theoretical analysis. This appears to be due to the assumption of a constant slope of the magnetization curve and the neglect of the armature reaction during the analysis.

The results indicate that, in general, a greater range of speed variation may be achieved through the use of a higher step up ratio R. This effect is also predicted by the analysis. However, a limitation is shown by examination of curves (c), (d) and (g) which correspond to the same output load T_o, but different step ratio R. Increasing R from R = 3.0 (curve c) to R = 4.92 (curve d) and to R = 6.41 (curve g) makes the characteristics (b) and (g) cross the ordinate which reduces the speed range. This appears to be associated with the generator running barely above its critical speed when the output speed is maximum, and hence, capable of significantly reduced range of energy dissipation over the entire range of R_L. The speed range of the system may thus be increased to a limit through a judicious increase in the step ratio R.

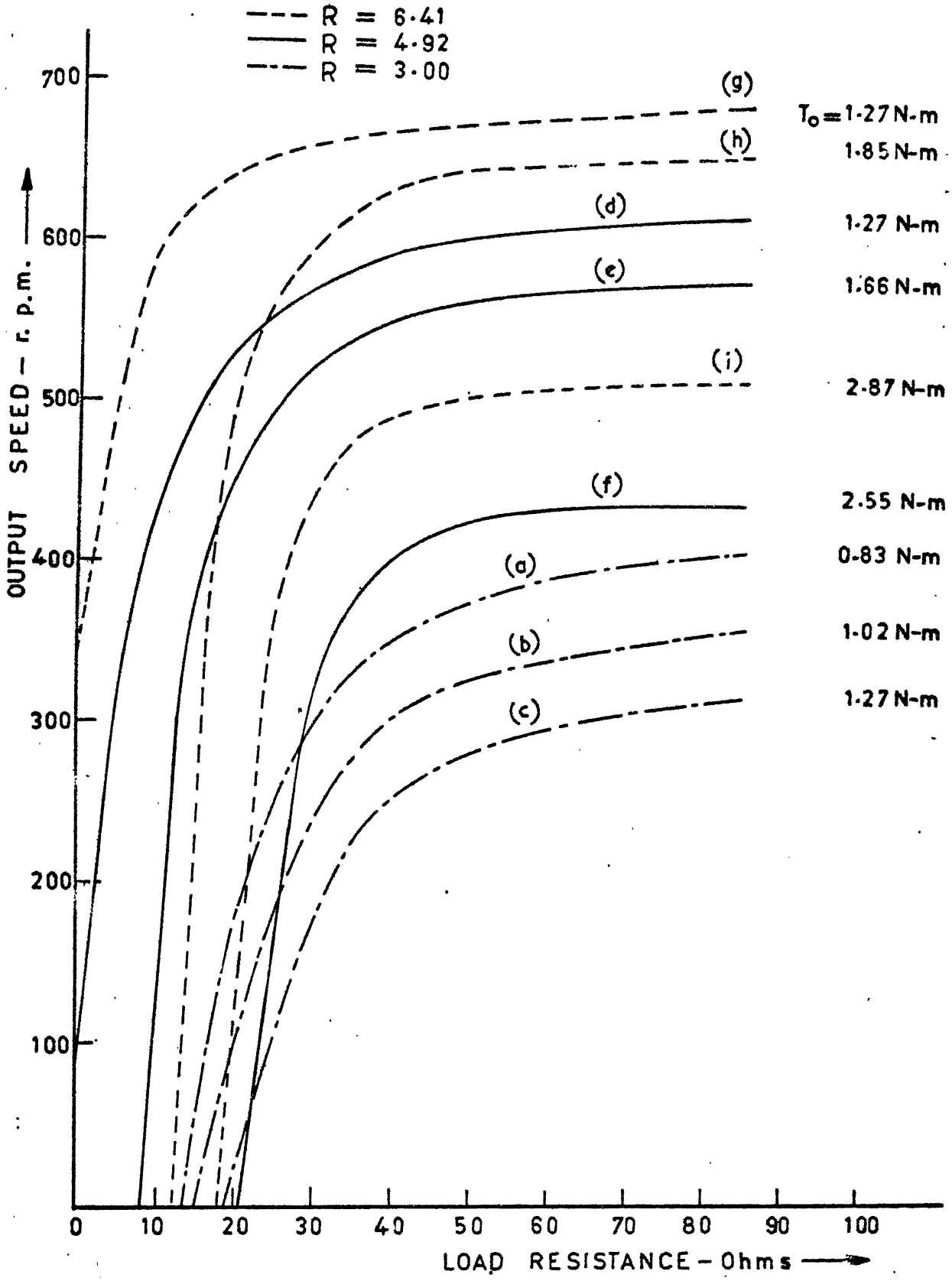

FIG. 3.3 EXPERIMENTAL $\omega_o - R_L$ CHARACTERISTICS OF THE SYSTEM.

CHAPTER 4

SUMMARY AND CONCLUSIONS

The development of a continuously variable speed drive system employing a mechanical differential and a dissipative control device is presented. The feasibility of employing three different physical systems, namely, (i) a ball governor, (ii) a mixing paddle and (iii) a dc shunt generator as control devices is investigated. The variations of the steady state output speed with control parameter are presented for all the three systems. The effect of output load variations on the system behaviour is examined. The dynamic behaviour of the mechanical differential gear-ball governor system is also studied. The possibility of improving the system speed of response through the selection of an optimum governor ball mass is explored.

An experimental set-up was fabricated to illustrate the practical feasibility of the proposed concept. A dc shunt generator was used as the control device because of the ease in fabrication. The plots indicating the variation of the output speed with load resistance are obtained for different values of the output load torque.

The main conclusions based on the present work may be summarized as :

(1) The proposed concept would be practical only for low power applications since a part of the input power is continuously dissipated in the control device.

(2) The analysis indicates that the differential gear-ball governor system has better performance characteristics compared to that employing a mixing paddle as the control device.

(3) The experimental results for the differential gear-dc shunt generator system show that the output speed changes due to variations in the output load. This does not agree with the theoretical prediction. The discrepancy appears to be due to the assumption of a linear magnetization curve and the neglect of the armature reaction during the modelling of the system.

(4) The experiment conducted with the differential gear-dc shunt generator system, however, establishes the practical feasibility of the concept for achieving a continuously variable output speed.

Experimental investigations of the system using the ball governor and the mixing paddle as control devices would represent an interesting future extension of the present study. Also, the development and analysis of other control devices, promising improved performance characteristics would be desirable.

REFERENCES

1. D.Z. Dvorak, ''Variable Speed Mechanical Drives'', Product Engineering, Vol. 34, pp. 63-74, Dec.23, 1963.
2. D.Z. Dvorak, ''Belt and Chain Drives'', Product Engineering, Vol. 35, pp. 91-97, Feb. 3, 1964.
3. Werner Holzbock, ''Which Hydraulic Drive'', Product Engineering, Vol. 34, pp. 63-76, April 15, 1963.
4. Baruch Berman, ''Variable Speed DC Drives'', Product Engineering, Vol. 33, pp. 58-67, April 2, 1962.
5. Baruch Berman, ''A.C. Adjustable Speed Drives'', Product Engineering, Vol. 34, pp. 81-89, July 8, 1963.
6. J.H. Rushton, E.W. Costich and H.J. Everett, ''Power Characteristics of Mixing Impellers - Part I'', Chemical Engineering Progress, Vol. 46, No.8, pp. 395-404, Aug., 1950.
7. J.H. Rushton, E.W. Costich and H.J. Everett, ''Power Characteristics of Mixing Impellers - Part II'', Chemical Engineering Progress, Vol. 46, No.9, pp.467-476, Sept., 1950.
8. Shinji Nagata, ''Mixing Principles and Applications'', John Wiley and Sons, New York, 1975.